12-31-2010

Design and Fabrication of a Membrane Integrated Microfluidic Cell Culture Device Suitable for High-Resolution Imaging

Alla Epshteyn
University of South Florida

Design and Fabrication of a Membrane Integrated Microfluidic Cell Culture

Device Suitable for High-Resolution Imaging

by

Alla A. Epshteyn

A thesis submitted in partial fulfillment
of the requirements for the degree of
Master of Science in Materials Science and Engineering
Department of Mechanical Engineering
College of Engineering
University of South Florida

Co-Major Professor: Joseph Cuiffi, Ph.D.
Co-Major Professor: Shekhar Bhansali, Ph.D.
Ashok Kumar, Ph.D.
Nathan Gallant, Ph.D.

Date of Approval:
October 22, 2010

Keywords: in vitro model, PDMS, substrate transfer, photolithography, layer by layer

Acknowledgements

Table of Contents

List of Tables

List of Figures

Abstract

Malaria remains a serious concern for people living and traveling to warm climates in Africa, Asia, and some parts of America. Understanding the mechanism of the malaria parasite in the liver phase could lead to important discoveries for preventative and treatment therapeutics before the disease develops into the blood stage. While in vitro liver cell culture models have been explored, a device that mimics the liver cell architecture with the capability of high-resolution imaging has never been created. In this research, a cell culture microfluidic device was designed and fabricated with a membrane integrated design to mimic the architecture of a liver, cell chamber dimensions affable for high-resolution imaging, and fluidic port design for optical access to both sides of the membrane for the study of malaria parasite invasion.

Chapter 1

Introduction

1.1 Background and Rationale

Malaria remains a critical public health problem worldwide, affecting 500 million and killing over 1 million people each year[1]. The disease continues to be a serious threat to people living and traveling to warm climates in Asia, some parts of America, and Africa (where the majority of the cases occur). Most commonly, malaria is transmitted to humans by a parasite, from a bite of an infected mosquito. The disease can also be transmitted through a blood transfusion or from an infected mother to her child during pregnancy.

The malaria life cycle begins with the natural infective stage, when sporozoites (parasite) release from an infected mosquito's salivary glands. Upon entering the body, the parasites migrate into the exoerythrocytic stage in the liver and invade hepatocytes, where they develop and multiply into the next form of the parasite, merozoites (Figure 1). Complete development of the exoerythrocytic stage results in the release of merozoites to the bloodstream, beginning the asexual erythrocytic stage. In the blood stream, the merozoites invade red blood cells where they mature, multiply, and rupture to infect more red blood cells. When a person's parasetemia (number of parasites in the blood) elevates, a fraction of the parasites are triggered to undergo gametocytogenesis. When a mosquito bites a human, the female and male gametocytes are

1

transferred through the bloodmeal. Inside the mosquito's gut, the gametocytes sexually recombine and carry on the life cycle of the parasite. The infected person develops fever-like symptoms and in more severe cases parasites released from the blood cells can lead to death.
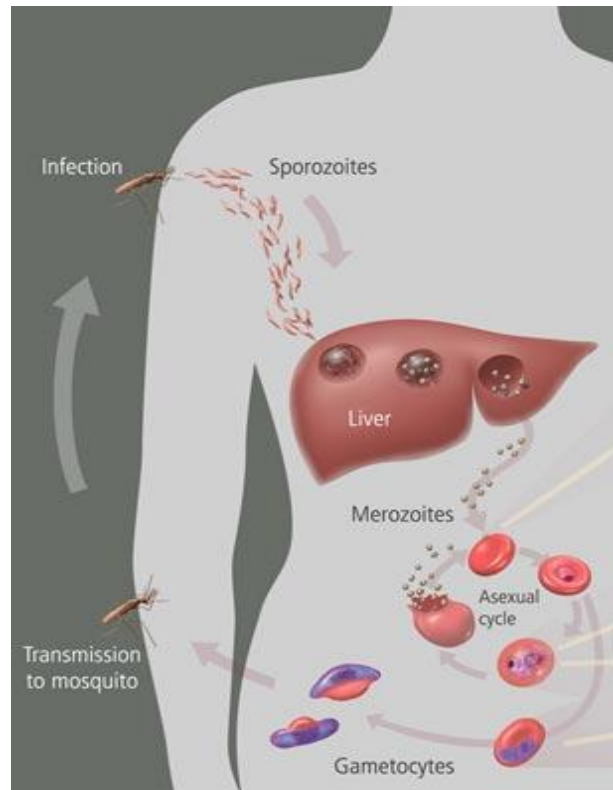
Figure 1- Life cycle of malaria development

Understanding the exoerythrocytic (liver) stage of malaria is essential to discovering disease cures because this stage is vital to the life cycle of the parasite. In addition, the parasite can remain dormant in the liver for up to 3 years before developing into the blood stage[2]. Very little is known about the dormant liver stage (hypnozoite) of the parasite and even visual identification and

2

documentation has been limited[3]. The entire invasion pathway (blood to liver to hepatocyte) is not fully understood. Understanding the liver stage parasite development could contain clues for effective antimalaria therapies.

Currently, the only clinically approved drug that treats the liver stage of the malaria parasite is Primaquine™. Due to pharmacokinetic limitations a patient has to take the drug 14 times a day for treatment to be effective[4]. More importantly, many patients cannot be candidates for the drug due to toxicity complications[5]. Limited research tools have hampered the advancement of liver stage malaria therapies.

Traditionally, clinical *in vivo* drug studies are performed on animals. However, in the case of malaria, while rodent parasite (*berghei*) *in vivo* models have revealed important parasite development insights, the human malaria parasites (*Plasmodium falciparum, Plasmodium vivax*) vary significantly from the rodent parasite strand[3]. Therefore, developing a human *in vitro* liver model of the parasite is imperative to discovering sufficient therapies to treat and prevent malaria.

The development of an *in vitro* liver stage malaria parasite invasion model for human malaria species, has been challenging due to the use of traditional cell culture systems. Monoculture approaches have been used to study *P. falciprum* with low infection rates measured by the number of infected hepatocytes compared to the number of sporozoites[3,6,7]. Low infection rates of the parasite may be attributed to the use of the traditional culture techniques that utilize flasks and Petri dishes, limiting the ability to recreate the cell-specific conditions vital for

3

cell development. Cells respond and grow based on its organ-specific micro-environmental conditions including shear stress, transport and diffusion of nutrients, and material interfaces[8]. Methods beyond traditional cell culture have been explored via co-cultures[9-12], micro-patterned cell arrays[12-17], and perfused systems[17-21] and have advanced *in vitro* liver models. However, to fully understand parasite development biology, further development is needed.

Numerous characteristics are important to consider when building a human liver stage malaria model. First, the re-creation of the cell architecture is important to studying the development of the parasite. Latest research suggests that the sporozoites travel through endothelial cells to enter its host cell, hepatocyte, in the liver. In addition to mimicking the cell architecture, a good model should consider the *in vivo* shear stress conditions of each cell type. For example, hepatocytes experience low shear stress (0.01-0.33 dyn/cm^2) because they line the static liver sinusoid[22-23]; whereas, endothelial cells are exposed to much greater shear stress (10-15 dyn/cm^2) attributed to the passing blood flow[24-25]. In addition considering shear stress, a relevant *in vitro* model should permit continuous perfusion of nutrients and gases to mimic the body's environment. Finally, the research platform must be developed within the working distance limitations of high-resolution optical microscopy (60X and up) to capture the tiny parasites (~1 X 3 μm). In summary, important considerations for developing a human *in vitro* liver stage malaria platform include mimicking cell architecture, shear stress, perfusion of flow, and the ability to take high-resolution images.

4

In this research, a microfluidic device was designed and successfully fabricated to study the malaria parasite invasion in a liver. The device will mimic the livers natural environment and aid in potential drug discovery. It will be shown through previous research that microfluidics serve to create more relevant *in vitro* environments than traditional culture techniques. The membrane integrated microfluidic concept will be presented for the application of creating a liver mimetic interface, which is essential for replicating the natural environment of the liver. The need for high-resolution microscopy will be described, along with important design criterion. The fabrication of the device will also be presented along with a novel substrate transfer technique, which can be used for creating three dimensional constructs. Finally, images of live cell culture in a device will be demonstrated as proof-of-concept for the successful device design capability to perform high-resolution images on both sides of the membrane.

1.2 Literature Review

1.2.1 Introduction to Micro-Fabricated Cell Culture Devices

The human body is composed of multiple organs, each one containing many types of cells. Each cell type experiences a unique environment based on the surrounding cells and organ location. The differentiation, growth and metabolism of a cell are highly dependent on the specific surrounding environment, which includes physical factors (e.g. temperature, pressure), chemical factors (e.g. pH, dissolved gas concentration) and biological factors (e.g. cytokines, extracellular matrix molecules). Adding to the spectrum of

5

variables, cell behavior can vary from person to person due to the variations in the genetic makeup of an individual. As an example of complex cellular environment within a tissue, the liver is composed of a lining of tightly packed hepatocytes followed by a space of Disse (Figure 2). On the other side are endothelial cells, Kupffer cells and the blood vessel. Micro-environment conditions in the liver include: local temperature, the spatial architecture created by the space of Disse, low shear stress surrounding the hepatocytes, the high shear stress experienced by endothelial cells due to the blood flow, and the continuous perfusion of nutrients and oxygen. The combination of some or all of the cells making up the liver as well as the architecture must be mimicked in order to create a biologically relevant *in vitro* liver model in a "dish".
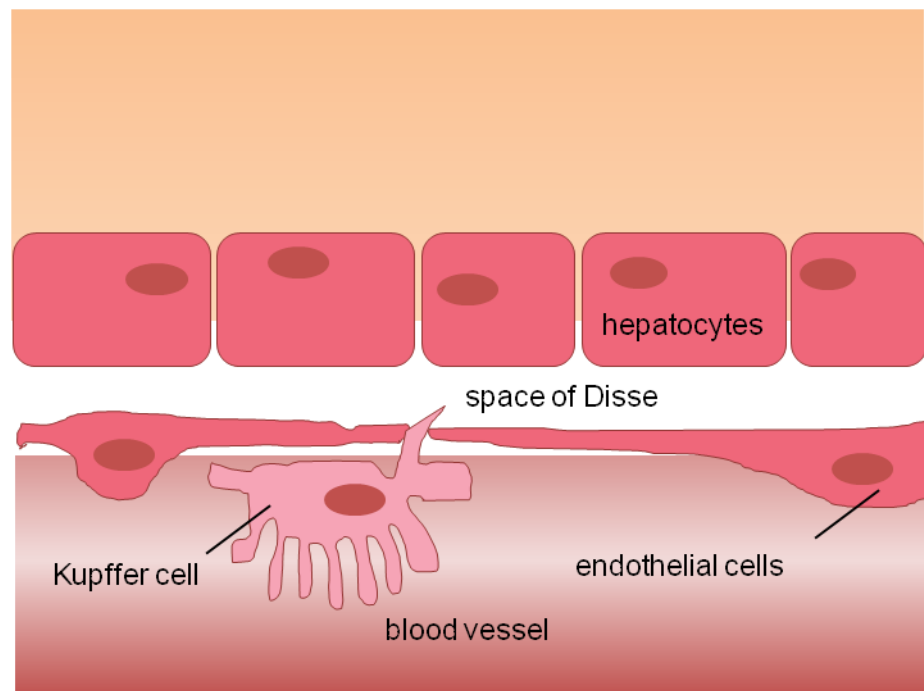
Figure 2- The cellular composition of the sinusoid of a human liver

With over a century of *in vitro* cell culture research, many research techniques have remained the unchanged. Cell studies have been limited to flasks, petri dishes, well plates, and glass slides[26]. The two dimensionality (2-D) of cell cultures, cell culture surface materials, and the inability to perfuse media are just a few important limitations of using traditional substrates in mimicking complex tissue organization. The monolayer growth of cells on a petri dishes' two dimensional surfaces significantly deviates from the body, a three dimensional intricate machine with exponential complexity[27]. Furthermore, these substrates are made out of a limited variety of materials that are typically relatively rigid (e.g. glass, polystyrene) unlike the body, which is composed of soft tissue, skin, muscle, and bones. Since a cell also responds to its mechanical surrounding cues, the surface environment provided by polystyrene dish can exhibit a surface roughness and mechanical stress that is not relevant to *in vivo* conditions[28]. Another limitation of using dishes and flasks is that during cell growth, media is introduced to the wells or the flask in a static batch mode[29]. After some time, the used media is removed from the substrate and a new batch is introduced to continue cell growth. Unlike the continuous flow and perfusion of nutrients in the body, a static culture system does behave like a relevant model of *in vivo* fluid flow.

The field of tissue engineering has emerged to address the limitations associated with materials, cellular architecture (2D vs. 3D) and static cell culture conditions[28]. While tissue engineering emerged from the need for regenerative medicinal applications, it has provided platforms for cellular level research. As an

7

example, the deviations of human responses to drugs from animal prediction studies are another driving force for the expansion of tissue engineering and the use of human *in vitro* models. Tissue scaffolds have been fabricated to mimic the extracellular matrix (ECM) for cell culture in various materials from plastics to biodegradable materials[30-32]. Patterned co-cultures have been shown prolong the phenotypic cell characteristics[12-17] of cells removed from the body. 3D hydrogels[33-34] have been used to provide a 3D cell culture scaffold, and microfluidic systems[26,36] have been used to study cells in a variety of materials and spatial geometries. All of the approaches, except for microfluidic devices, do not address the limitations of static cell culture, a vital requirement for transport phenomenon of cell nutrients. Microfluidics offer unprecedented control over traditional cell culture systems by providing spatial complexity and continuous perfusion of nutrients and gases.

Microfluidic technology is a general term for the manipulation of small volumes of fluids (10^{-9} to 10^{-18} liters) by machining micrometer scale features[38]. Microfluidic studies have become widespread in research laboratories using photolithography, a process utilizing UV sensitive material to create micro patterns. Kumar *et al* cured a polydimethylsiloxane (PDMS) material over a micro-patterned wafer to yield a negative mold, a process now known as soft photolithography[40]. The feature scale of microfluidic devices allows for the recreation of many important *in vivo* conditions including increasing the cell surface area to extracellular fluid ratio, continuous perfusion of nutrients, diffusion of gases, flow-induced shear stress effects, surface adsorption, and effective

8

culture volume[41-41]. Many microfluidic systems have been studied for applications in cell culture. *In vitro* models of liver[43], muscle[44], brain[45,46], bone[47] and lung tssue[49,50] have been recreated in microfluidic systems. The differentiation of stem cells by manipulation of the microfluidic environment has also been studied[48]. In addition, microfluidic systems have been useful for studies of cell separation[51], cell adhesion[52], sensor development[38,39], and on-chip assays[35,37].
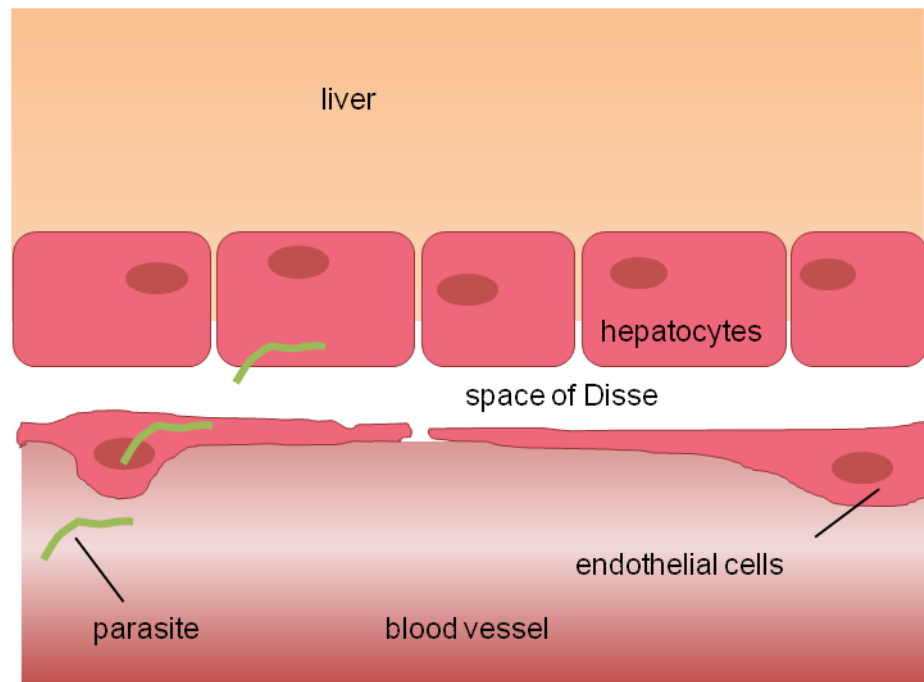
Figure 3- The malaria parasite is believed to travel from endothelial cells through space of Disse into the hepatocytes

Liver *in vitro* cultures have been a significant focus in research because drugs often fail clinical testing due to their effects on the liver[12,53-56]. Liver *in vitro* models are particularly important for the development of therapeutics for the liver stage malaria parasite invasion. The parasite infects the liver by first entering the

9

bloodstream from a mosquito bite. It then passes through the endothelial and space of Disse layers in the liver sinusoid (see Figure 3) to infect a hepatocyte. Current *in vitro* liver models are limited in their correlation with this cellular architecture, and therefore, have provided limited infection rates and improper parasite development. This work focuses on a cell culture device, building on the efforts of reported work reviewed below, to recreate some of this architecture, hopefully providing microenvironmental features in order to properly study malaria infection.

1.2.2 Micro-Patterned Co-Culture Techniques

Khetani, *et al* patterned cellular co-cultures in an organized array and found an optimal combination which sustained a liver culture exhibiting standard hepatocyte activity for several days[12]. They reported the maintenance of primary hepatocyte characteristics with a cellular co-culture of fibroblasts. The study did not include other important cell types such as endothelial cells, and the system lacked a perfused nutrient supply.   Furthermore, the architecture of the true *in vivo* micro-environment was not mimicked as the cells were cultured side by side on a flat plate, not stacked in "layers" as they are found in the sinusoids (Figure 2). These limitations are especially important given the specific application of malaria invasion because the parasite must pass through the endothelial barrier to get to the hepatocytes. In follow-on work[15] the authors added endothelial cells to the co-culture mix. While the system was improved, the work still did not address the perfusion of nutrients or the architecture of the sinusoid.

10

Recent work presented a method to generate layered micro-patterned hepatocyte-fibroblast co-cultures which increased the heterotypic cellular interface[16]. This research further improved the *in vitro* liver co-culture model with structural cell culture composition that more closely mimics the layers in a sinusoid, but important features were not included. The system lacked endothelial cells, which are required for the malaria infection model, and the co-culture stack model lacked nutrient perfusion.

In another study, the authors developed a perfused chamber over a patterned co-culture substrate with continuous nutrient flow[17]. Although media flow over the hepatocyte cell culture provided a continuous supply of the nutrients and gas, the flow also exposed the cell culture to high shear stresses unlike the low shear stresses experienced in *in vivo* conditions. In addition, this research still did not address the cell architecture of the liver sinusoid.

All the co-culture liver models to date have addressed some partial combination of inclusion of important cell types, generation of the true 3D structure of the sinusoid, and perfusion of nutrients. Still, none of the systems address all three factors in one platform, requiring further development of a more relevant *in vitro* model.

1.2.3 Membrane-Integrated Techniques

Membrane-based cell culture systems emerged from the use of membrane inserts placed in multi-well plates (e.g. Millicell®, Millipore Inc., Transwell®, Corning Inc.) because they easily integrate into traditional cell

11

culture technique protocols. The static membrane insert culture technique has proven effective for a variety of tissue models[57-58], but it is limited as a micro-environmental construct due to the absence of flow. This has led to a variety of microfluidic approaches using either horizontally integrated membrane layers[59-62] or vertically defined features to create a membrane or barrier[56,63].

Successful microfluidic cellular constructs with different cell types seeded on opposite sides of the membrane have been demonstrated for models of the alveolar-capillary interface[49,50], smooth muscle cell-endothelial interface[59], and blood-brain barrier[60]. Furthermore, constructs with cells seeded on only one side of the membrane have been used to study endothelial layer permeability[61], mimic an endothelial barrier and protect shear sensitive hepatocytes from perfusion[18,19], and optimize perfusion conditions for renal tubular cells[62]. Although vertically defined membranes are more suited for optical interrogation of the cells on either side of the barrier, they lack the large surface area possible in horizontal configurations, which is important for studying chemical transport and cell or pathogen migration from one cell layer to the other. While all of the described membrane models have been suitable for their respective cell studies, they do not allow for high-resolution optical access to both sides of the membrane, necessary for our specific desire to observe a parasite invasion.

Membrane integrated perfused systems have been used to study liver *in vitro* models. Carraro *et al* reported on a membrane integrated dual chamber system which allowed for selective seeding of hepatocytes on one side of the membrane and perfusion of media flow on the other side of the membrane[18].

12

Advancements of this model include membrane integration for mimicking liver sinusoid architecture and perfusion of nutrient flow. However, the model lacked the incorporation of endothelial cells, which are important for the malaria infection model because the parasite enters liver through the invasion of endothelial cells. Furthermore, the system was not capable of high-resolution imaging and was not designed for multiplexing, which are required for studying parasite infection and for drug screening.

A recent implementation of a membrane device as a lung *in vitro* model is a system that is useful to relate to the creation of a malaria liver model. The team developed an *in vitro* lung model for monitoring neutrophil migration through the membrane[50], similar to the application of studying parasite migration through the membrane. The device construction allowed for adequate visualization of whole cells. However, this specific malaria study requires higher resolution sub-cellular imaging to observe and study the small ~1 x 3 μm parasite. Therefore, a thin layer device, which accommodates the short working depths of high-resolution optics, must be developed to adequately study malaria parasite infection.

While liver cell cultures for malaria have been reported, live cells have never been seeded on both sides of a membrane in a perfused system, which may provide the proper microenvironmental factors to improve parasite infection and development, which is necessary for a practical model. Furthermore, no cell culture system has ever combined 1) a membrane, 2) perfusion, and 3) potential for high-resolution live-cell imaging on either side of the membrane into one device. The culture device described in this manuscript, which combines these

13

three features, was designed for the potential of high throughput drug testing with no modification necessary to microscope imaging systems. The design, fabrication, and testing of this ultra thin membrane integrated device amenable to high-resolution microscopy, will be described in the following sections.

Chapter 2

Device Design

2.1 Device Concept

A membrane integrated microfluidic device was designed to study the pathway of the malaria parasite into the liver. Currently, the parasite is believed to travel from endothelial cells through the space of Disse into its host cells, hepatocytes for further development[3]. To mimic the cell architectural structure of the liver, a dual chamber microfluidic device was designed for selective seeding of hepatocytes on one side of the membrane and endothelial cells on the other, with the membrane mimicking the space of Disse (Figure 4).
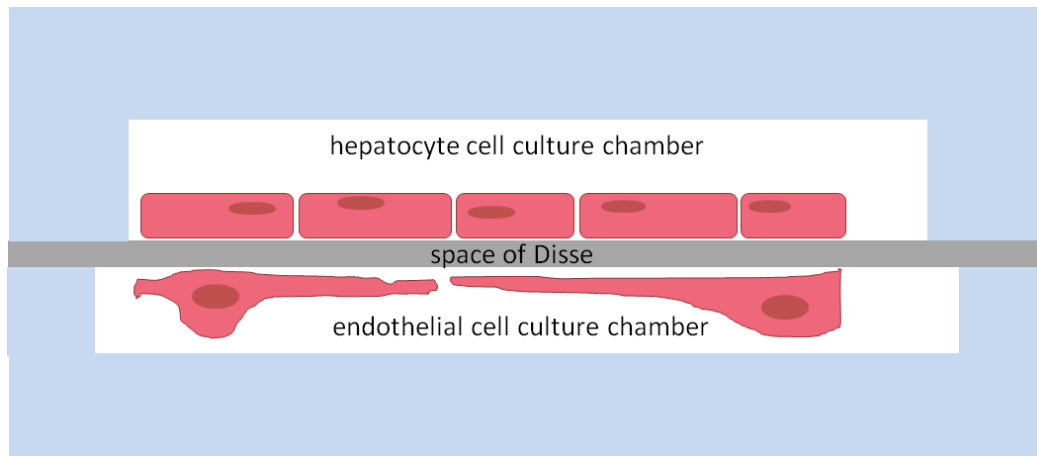
Figure 4- The cross section view of the device design mimicking the liver sinusoids architecture

In addition to addressing cellular organization of the liver environment, this *in vitro* model addressed cell specific shear stress conditions and allowed for perfusion of nutrients. Figure 4 shows the isometric view of the device concept illustrating a membrane sandwiched between the top cell chamber (red) and the bottom cell chamber (blue). The device was designed to perfuse media through the endothelial chamber exposing the cells to shear stress. The flow could be static in the hepatocyte chamber to protect the cells from shear to mimic the conditions of the liver sinusoid. The choice to utilize a membrane-suspended microfluidic device enabled the control of separate cell culture micro-environments.
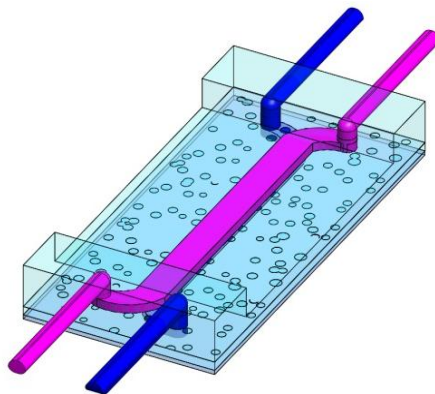
Figure 5- Top view of the device design showing the flow into the top (red) and bottom (blue) cell chambers

The device dimensions were also designed to accommodate high-resolution optical microscopy necessary to image the parasite infection. Other requirements for the microfluidic device included continuous media perfusion, optimal gas permeability, and the ease of selectively seeding cells on opposite sides of the membrane for the recreation of the parasite invasion in the liver

16

environment. Device dimensions, choice of material, and the fluid port design were some of the factors that accounted for achieving the aforementioned design criteria.

2.2 Material Selection: Prototyping with PDMS

An optimal organ mimetic microfluidic platform has appealing characteristics for dynamic high-resolution microscopy, cellular proliferation, and differentiation. Cell seeding surfaces in microfluidic devices include plastic, glass and metal substrates. Metal substrates and some plastics are limiting to microscopy since light cannot go through hundreds of micrometers of material and therefore, transparent plastics and glass are preferentially chosen. Common prototyping plastics can be arranged in 3 categories: thermosets, thermoplastics, and elastomers[64]. Thermoset polymers cure under radiation, such as UV light, and have deformation temperatures close to glass transition temperatures. Polyimide and SU-8, an epoxy based negative photoresist, are examples of thermosets. They can be manufactured by standard microfabrication techniques that involve casting, lithography, and etching[64]. Out of the 3 polymer types, thermosets are the least transparent, most expensive, and most difficult to fabricate with two-dimensional features. Thermoplastic polymers soften upon heating and have a large difference between the deformation and the glass transition temperatures. Examples of thermoplastics include Poly (methylmethacrylate) (PMMA), Poly (carbonate) (PC), and Poly (etheretherketone) (PEEK) all of which can be fabricated via injection molding[65],

17

hot embossing, thermoforming, or laser ablation. The last category of polymers is elastomers, which can stretch to at least 200% of its length and relax back to the original shape[64]. Polydimethylsiloxane (PDMS) is a Si based elastomer that can be microfabricated by casting, lithography and etching. Elastomers, such as PDMS have a high optical transparency, are economical to produce, and can be prototyped more conveniently than thermoplastic polymers[64].

Poly (dimethylsiloxane) (PDMS) is the most common prototyping material for microfluidic systems because of its attractive properties in ease of fabrication reproducibility, light transparency, and high permeability to small molecules like H_2O and CO_2, the control of which is vital to performing successful cell studies[66]. When cured over a patterned platform, PDMS can replicate the roughness of the surface down to nanometer size features[40]. Thus, desired features can be successfully replicated into PDMS by patterning a molding substrate. Another advantage of using PDMS as a prototype material is that molds from PDMS-to-PDMS may also be replicated. Thus, both the negative and the exact replicate of a mold can be fabricated from the original patterned substrate using PDMS.

PDMS exhibits desirable optical properties for dynamic cell imaging. PDMS has low autofluorescence[67], which enables fluorescence imaging throughout the device with minimal interference. With PDMS, the only significant limitation of microscopy roots from the microscope itself and its working distance parameters. Elastic properties of PDMS, which can be varied through the polymer thickness, enable construction of organ mimetic microfluidic models[50]. Cell growth can be promoted in microfluidic devices using existing standard

18

substrate surface treatments[68]. Common surface treatment techniques include plasma exposure for hydrophilicity enhancement and protein coating to promote cell adhesion and growth. The overall optical characteristics, biocompatibility, scalability, and flexibility of PDMS make it attractive to build organ mimetic microfluidic constructs.

2.3 Device Layout

Since this device was developed for the application of studying liver stage malaria parasite invasion, high-resolution microscopy accommodation was an important design criterion. For optimum high-resolution optics, cells are typically observed on the opposite side of a glass coverslip using an inverted microscope setup. Therefore, the device concept started with a cell chamber, built with an included membrane, bonded to a glass cover slip.
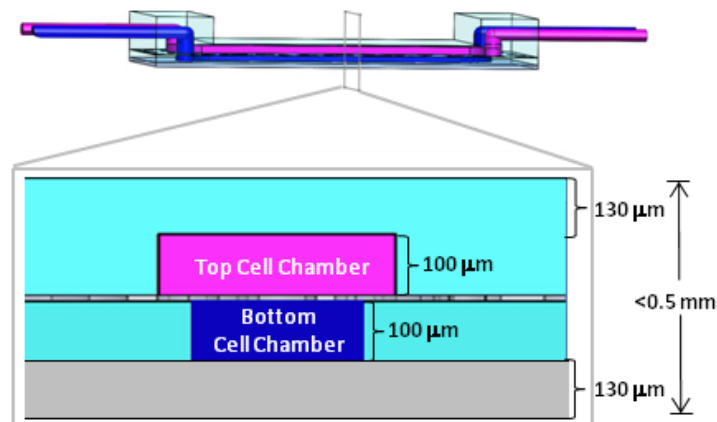
Figure 6- Side view of the membrane-integrated design affable for high-resolution optical access to both sides of the membrane

This device required high-resolution optical access to both sides of the membrane to observe the malaria parasite from one side of the membrane or the other. Consequently, the geometric configuration of the cell chambers on both sides of the membrane aimed at addressing working distance limitations of high-resolution microscopy. In a standard inverted microscope, the working depths are limited to an additional 130-200 µm past the standard No. 1½ glass cover slip; therefore, the device was designed with a 100 µm tall cell chamber space between a glass coverslip bottom and the membrane (Figure 6). Next, a matching 100 µm tall cell chamber space was placed over the membrane, followed by an additional 130-200 µm of cover material (Figure 6). Thus, high-resolution access to both sides of the membrane was allowed by considering the working depths limitations of a standard inverted microscope.
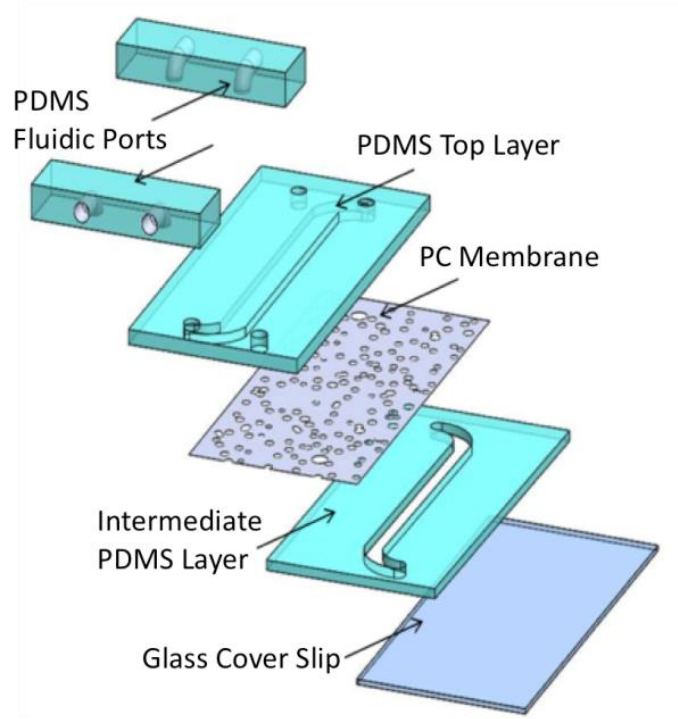
Figure 7- Exploded view of device components

20

The device was designed to be composed of 4 layers: a glass coverslip at the bottom, an intermediate PDMS layer, a Polycarbonate (PC) membrane, and PDMS layer on top as shown in (Figure 7). The coverslip on the bottom provided mechanical support and allowed for high-resolution microscopy, while the thin intermediate and top PDMS layers allowed for gas exchange. The membrane type and channel widths were chosen based on prior work[59] and ability to tailor the surface chemistry for cell culture. Here, a track-etched PC membrane (10 μm thick, 10 μm pores) was incorporated into the device. Lastly, a frame adapter was designed to view the membrane from the top or the bottom of the device and to organize tubing, see Figure 8.
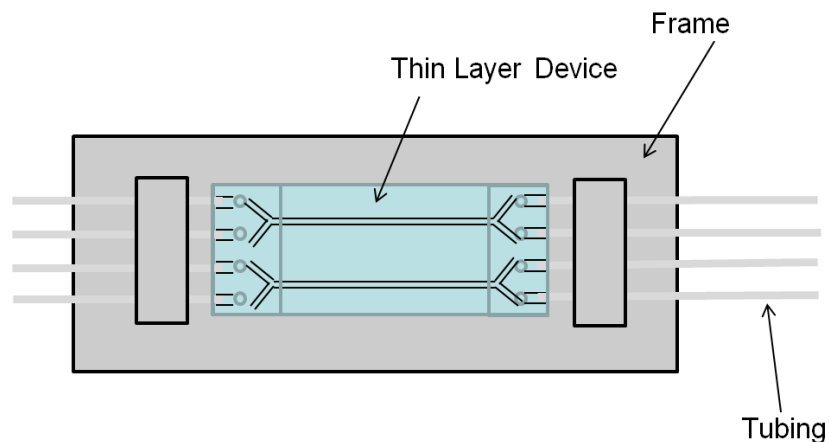
Figure 8- Top view of a single chip designed with two independent devices

Straight channels were chosen for the chambers on the top and bottom of the membrane to accommodate for the ease of seeding. The width of the channels was chosen to be 500 μm based on a previously optimized perfused membrane hepatocyte system[59]. Because high-resolution objectives typically have a diameter of 22-30 mm with a shallow radial slope away from the lens, the

21

channel length was chosen to be 50 mm long. The channel layout was designed with two independent devices on a glass cover slide to demonstrate the potential for multiplexing. Figure 8 shows one chip with 2 devices where the red represents the fluid flow into the top cell chamber and the blue represents the fluid flow of the bottom cell chamber.
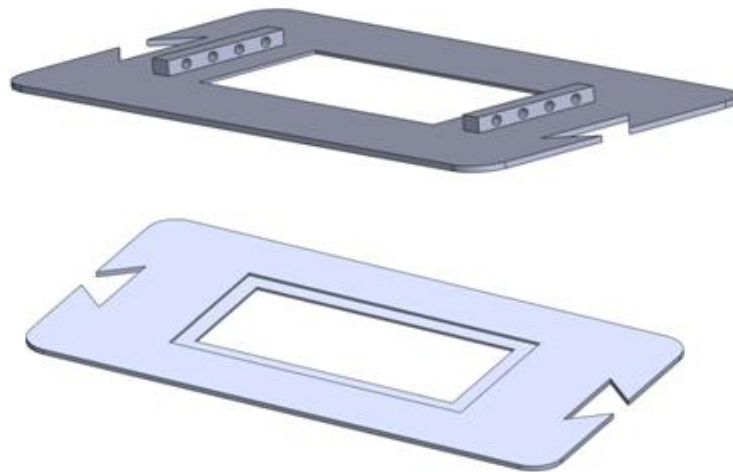
Figure 9- SolidWorks^{TM} drawing for the device holder top and bottom custom designed to fit into a microscope stage

One design component for device development was customizing a chip holder to fit into a microscope stage. SolidWorks^{TM} was used to design the holder in two parts: top and bottom with the overall goal to fit into a microscope stage and be able the flip the chip upside down for optical access to both sides of the membrane (Figure 9). The bottom part of the holder utilized a recessed space matching the chip thickness and surface area for localizing the chip. The top of the holder added structure for the tubing connections. Finally, both the top and

22

the bottom parts were designed with a compartment to help organize the tubing. Overall, the device holder provided structural integrity for the thin chip, robustness to the tubing connections, organization to accomodate the high throughput design, and most importantly allowed the device to be flipped upside down for optical access to both sides of the membrane.

2.4 Fluidic Interconnects
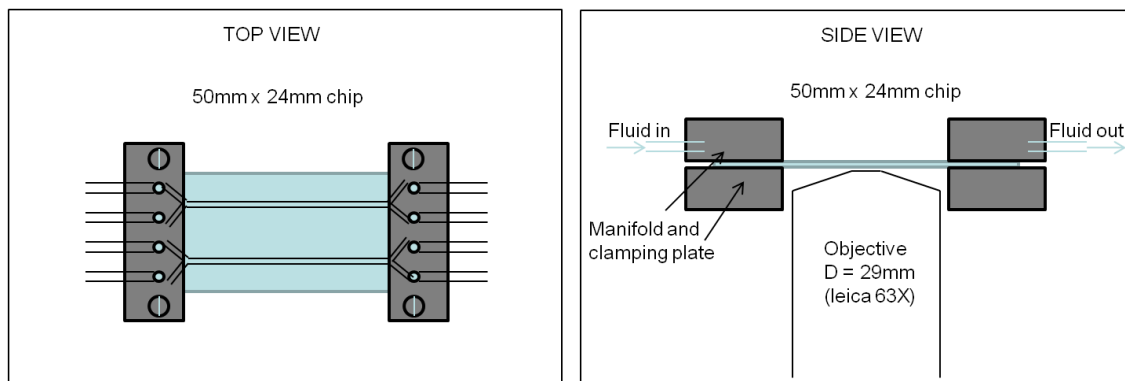
Figure 10- Traditional clamp manifold design for fluidic port accommodation

Once the membrane model was chosen and channel dimensions were designed to accommodate for high-resolution access and media perfusion, the fluidic ports had to be designed. The first design for the fluidic port inlets utilized a clamp manifold (Figure 10). Multiple disadvantages to this traditional manifold led to the redesign of the concept. In the traditional manifold method, bulky material over the channel inlets on top of the chip were matched with a securing material underneath the chip, and the two components were tightened by screws or clamped. Clamping material on the bottom of the chip limited lateral movement

23

of the objective. In addition, since the device was designed to be flipped for optical access to the top of the membrane, the clamping material on top of the chip restricted the high-resolution objective movement as well. By limiting the objective movement, optical access to the channel area was restricted. In addition, the glass coverslip bottom often broke during clamp fastening. Lastly, aligning the micro-scale fluidic port on the chip to the manifold ports was extremely challenging during the clamping process. Overall, microscopy limitations, device fragility, and alignment challenges necessitated development of another manifold approach.
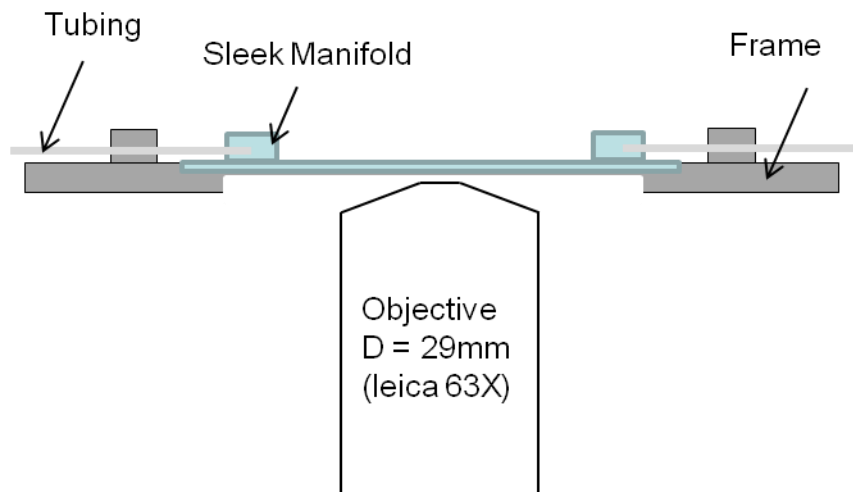
Figure 11- Features of the low profile fluid port design

To accommodate for all of the clamp manifold restrictions on the fluidic port, a low-profile port was designed utilizing an extension material and a support frame (Figure 11). Arguably the most significant improvement to this design was the removal of manifold material underneath the chip. With no barriers on the

24

bottom of the chip, the inverted device in frame would not be limited laterally, making the entire channel area accessible for microscopic visualization. The top material of the frame was also minimized from the clamp design. When the chip was inverted to access the top of the membrane, the newly added manifold material did not interfere with the optical access because of its minimal size. In addition, because the PC membrane was translucent, the cell chamber on top of the membrane was accessible through the bottom glass cover slip since it was in the limits of the working distance of the high-resolution objective. Aligning issues were also eliminated with the new fluidic port design since the extension material was designed to bond to the chip before tubing and support frame were added. This extension material was fabricated to be compatible with commercially available fluidic components like tubing, syringe tips, and fluid fittings. Finally, the frame component of the fluidic port design provided structural robustness for the chip, tubing organization, and the ability to integrate the device right side up and upside down.

Overall, a novel microfluidic cell culture device with a horizontally integrated membrane amenable to high-resolution live cell microscopy on either side of the membrane was designed. In addition, the fluidic port design eliminated any objective movement restriction, improved robustness of the chip, and provided high-resolution optical access to the entire top and bottom of the membrane. While the channel dimensions and membrane design were designed to accommodate a specific application in capturing the invasion of a malaria

parasite into the liver, the geometric dimensions can be tailored for various cell culture studies.

Chapter 3

Device Fabrication

3.1 Component Fabrication

With the design of the device optimized, the fabrication plan included the fabrication of each layer component, assembly, and bonding optimization. Finally, fluidic connects were fabricated and a device mounting frame was rapid prototyped. Not every component layer had to be fabricated: the 130 μm glass cover slip bottom (No. 1) was purchased from Corning, and the PC membrane was purchased from GE Osmonics with 10 μm pores and ~ 10 μm thicknesses. The top PDMS layer, intermediate PDMS layer, and the fluidic ports were each fabricated separately utilizing three different soft photolithography techniques respectively: spinning, lamination, and casting. Soft photolithography refers to the process of curing a polymer over a patterned substrate which results in a negative polymer mold (Figure 12)
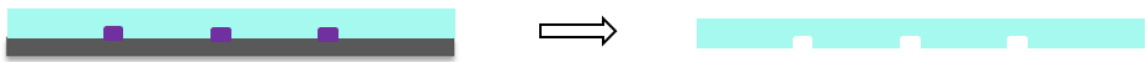
Figure 12- Soft photolithography demonstration

Standard photolithography methods were used to create the micropatterned wafers for PDMS molding. Photolithography is a process where a polymer (photoresist) is cross-linked upon the exposure to UV light through a

27

selectively patterned mask creating a micro-patterned substrate (Figure 13). To fabricate micropatterns with a height of 100 µm, 3050 SU-8 photoresist (Microchem Inc.) was chosen since the feature height was within the thickness limitations of the polymer. A separate mask pattern was designed to mold each PDMS device component. In the case of the spin layer pattern, the wafer was designed with 2 devices per chip to demonstrate potential for multiplexing and 2 chips per wafer for accelerating component fabrication (Figure 13e). For each soft photolithography process, Sylgard 184 PDMS (Dow Corning) was mixed at 10:1 ratio of polymer base to curing agent and then degased in a vacuum chamber for 1 hr or until all bubbles were removed. However, before the PDMS could be molded, the patterned wafers had to be fabricated and then surface treated.
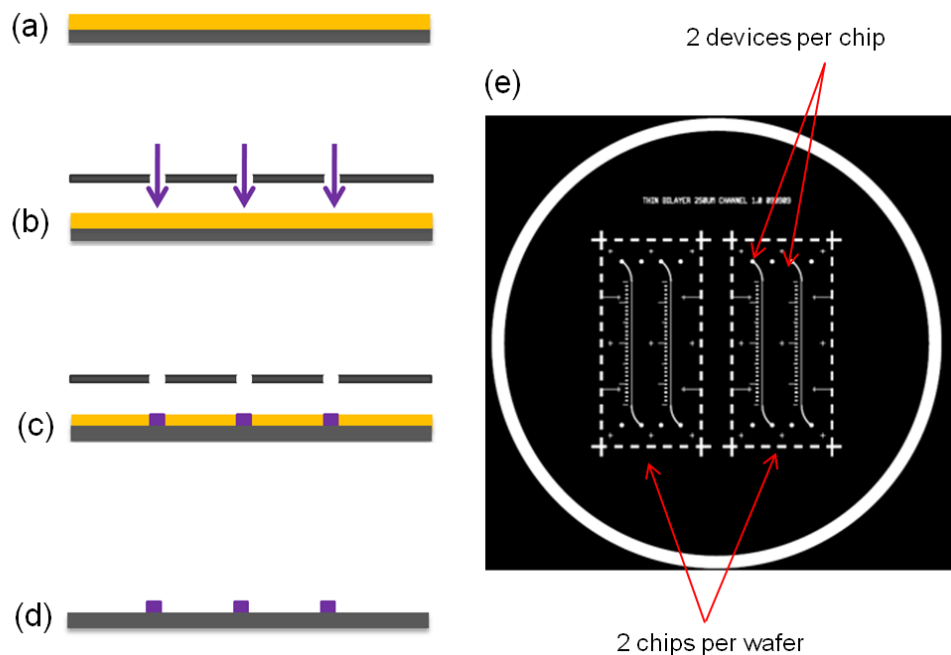
Figure 13- Summary of the photolithography process

Each wafer mold was fabricated by first spinning 3050 SU-8 photoresist on a silicon wafer (100 mm wafer diameter, 500 µm thick) to the desired feature height of 100 µm. The process started with wafer cleaning steps: 5 min of an isopropanol (IPA) rinse, 5 min of a DI water rinse, 5 min of dehydration at 200 °C, and finally, 2 min cooling using nitrogen (N_2) gas. Next, ~10 mL of 3050 SU-8 was spun at 500 RPM with acceleration of 84 RPM/s for 10 s, followed by 2000 RPM with acceleration of 336 RPM/s for 30 s (Figure 13a) to reach a target thickness of 100 µm. The wafer was then heated (soft baked) at 95 °C for 20 min and cooled at room temperature for 3 minutes. Next the SU-8 covered wafer was exposed to UV light through the transparency at light intensity of ~27.5mW/cm^2 on a Karl Suss MA 56 for 30 seconds (Figure 13b). The mask for the top PDMS layer is shown in Figure 13e. A post exposure bake followed the UV exposure first at 65 °C for 1 min, then at 95 °C for 5 min, and cooled for 3 min at room temperature. Finally, the photoresist was submerged and aggravated in SU-8 developer (Microchem Inc.) for ~8.5 min, rinsed in IPA for 30 s and dried with N_2. The unexposed resist developed away, resulting in a micropatterned wafer (Figure 13d).

Once the wafer molds were fabricated for each PDMS component, they were surface treated to prevent PDMS from sticking to the wafer. Tridecafluoro-1,1,2,2-tetrahydrooctyl) trichlorosilane is a common chemical wafer pre-treatment for soft photolithography applications[69]. With this technique, the wafer is placed into a chamber along with a glass coverslip. A total of 5 µL of the trichlorosilane (Gel-Est) was measured on to the glass coverslip. Next, vacuum suction is

29

applied to the chamber for 30 min while the silane is vapor deposited on the surface of the wafers.

After the wafers were surface treated, the top PDMS layer was fabricated using a spinning process (Figure 14). In a spinning technique, a patterned wafer is placed on a spin chuck and uncured polymer is poured over the wafer. The chuck is then spun at a programmed recipe, distributing the polymer over the wafer. The speed at which the chuck rotates determines the thickness of the polymer product. For this device, 10 g of uncured PDMS was spun at 650 RPM for 1 min. Multiple spins were used to build up the thickness of the polymer. For the top PDMS layer, the polymer was cured after the first spin and then another 10 g of uncured PDMS was spun at 650 RPM for 1 min. Two spins were required to achieve a uniform 230 μm (Figure 6) thickness over the wafer surface area. After the second PDMS layer was cured, the polymer sheet was peeled off of the wafer and trimmed as necessary for assembly.

The PDMS bottom layer required opened pattern features so it was fabricated utilizing a previously reported lamination technique[70]. In lamination, uncured polymer is poured over a patterned wafer in a chamber and a piston pushes down over the polymer/wafer stack, applying a uniform load. With added heat, the polymer cures to the height of the tallest wafer mold features resulting in a punched through patterned polymer film (Figure 14). The standard procedures reported optimal lamination at 65 °C with 20 psi of pressure. However, in the case of fabricating 100 μm thick bottom PDMS films, features across a macro surface area often resulted in inconsistent thicknesses using the

30

standard lamination protocol. Laborious modifications were required to produce a protocol resulting in high yield of punched through 100 µm PDMS films. PDMS volume was optimized because excess of polymer hindered laminating through the film, and too little PDMS would result in bubbles in the polymer film. An additional spinning step was added to spread out the minimal PDMS over the wafer mold before placing the stack into the laminator.
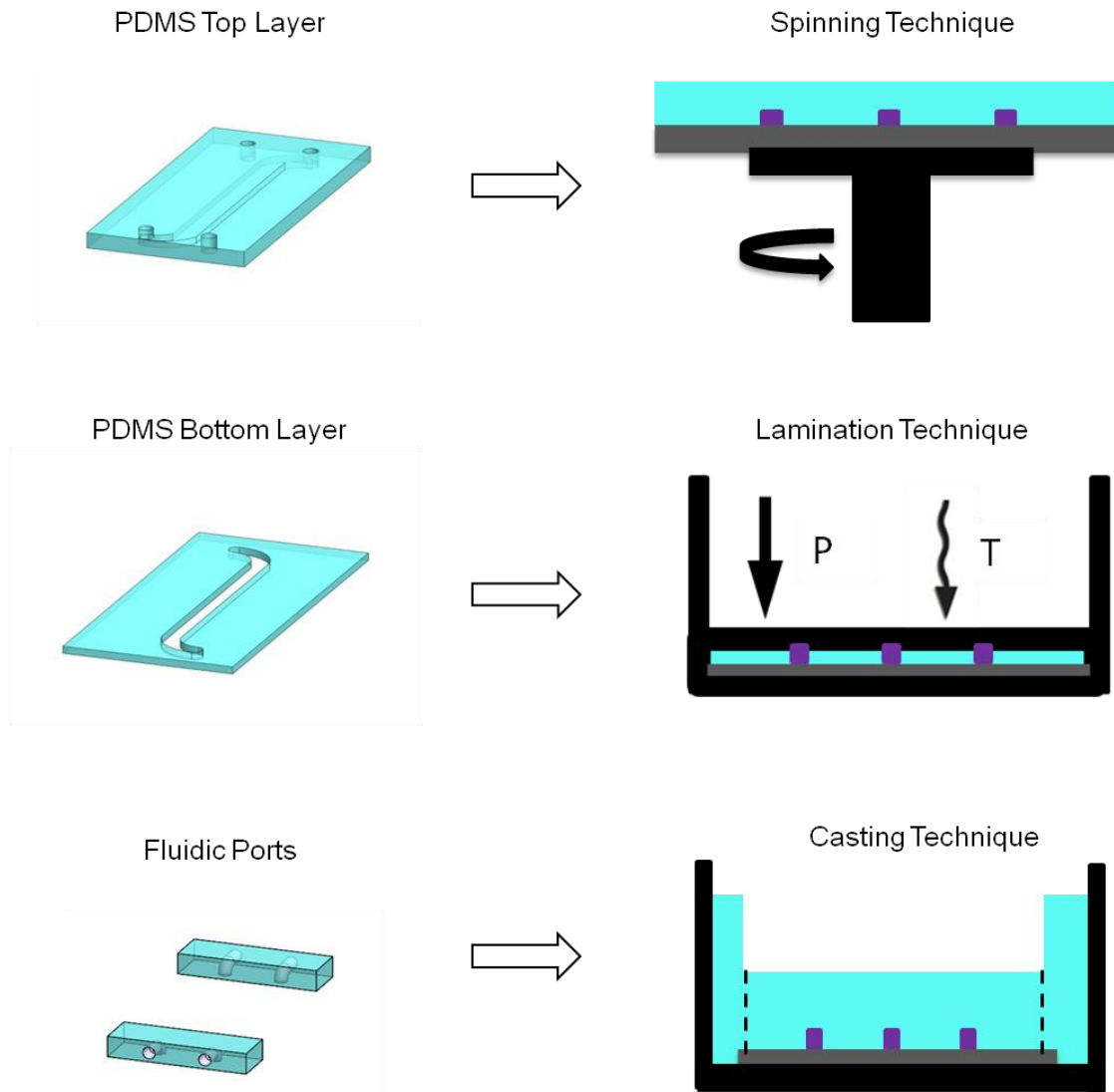
Figure 14- The bottom and top PDMS channel layers, and the fluidic ports were each fabricated using 3 separate photolithography techniques

Figure 15 shows the modified lamination steps for optimized fabrication of the bottom PDMS layer. First, the patterned wafer was trimmed into 2 separate chips to fit in the chamber. Next 1.8 g of degased PDMS was poured over the wafer chip (Figure 15a). The PDMS had to be degased again for 30 min or until all bubbles were removed. Next, to distribute the PDMS evenly, the wafer chip was spun at 600 RPM for 45 s (Figure 15b). The wafer was then moved to the lamination chamber, where kapton was carefully placed on top of the uncured PDMS (Figure 15c). To deposit the kapton over the uncured PDMS without forming any bubbles in the polymer, kapton was held with one edge bent upward and released down slowly across the mold. Finally, the chamber was closed on top of the stack and cured at 65 °C and 40 psi for 25 min (Figure 15d).
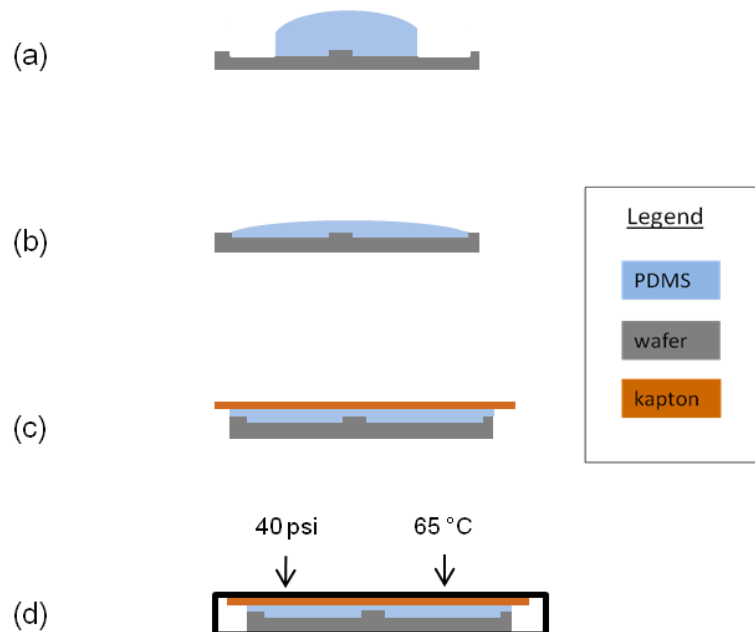
Figure 15- Lamination steps for bottom PDMS layer fabrication

Finally, the fluidic ports were fabricated using a casting soft photolithography technique. In casting, PDMS is poured into a well with a patterned wafer bottom. The amount of PDMS poured on top of the wafer determines the thickness of the resulting mold, see Figure 14. A wafer patterned with multiple fluidic manifolds was used to cast 15 g of PDMS. Individual manifolds were trimmed and inlets were inserted with a biopsy punch. Biopsy punch diameter, 1.5 mm, was chosen based on the tubing outer diameter, also 1.5mm; which was eventually inserted into the fluidic ports.

3.2 Substrate Transfer Technique

While the lamination procedure (Figure 15) was optimized to produced PDMS films with laminated through features; transferring the thin PDMS film for the assembly process proved to be very challenging. Because the PDMS bottom layer geometric configuration was thin (100 μm) and had a surface area of a 24 mm by 50 mm, the bottom PDMS layer was not free-standing and therefore difficult to handle (Figure 16a). In addition, when disassembling the lamination set up, the PDMS often did not lift along with the kapton and remained on the wafer. Removing the PDMS thin film from the wafer substrate created stretching of the PDMS film, and thus was not able to be picked up transferred for layer assembly with the thin PDMS form (Figure 16b). Even if the PDMS lifted off with the kapton, the structure of the PDMS stretched and deformed in the channel dimensions, critical features for final device use (Figure 16c).
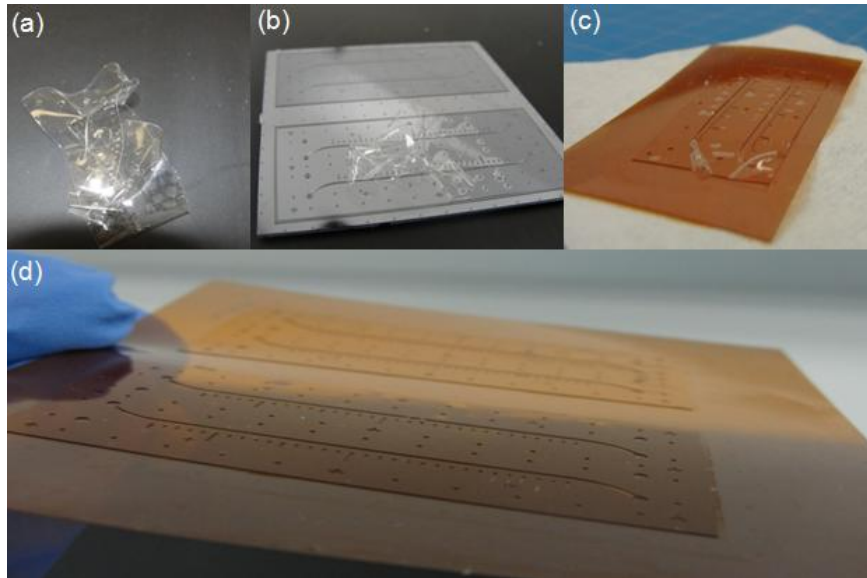
Figure 16- Substrate transfer technique addressed challenges with transferring thin PDMS film from wafer to Kapton

To address the difficulties handling laminated thin PDMS layers, a substrate transfer technique was discovered to enable the transfer of a thin PDMS layer from the wafer to a kapton film. This technique eliminated any feature distortion or structural deformation by transferring each molded piece onto a carrier material during assembly. For this technique, kapton was treated with oxygen (O_2) plasma before placement on top of the uncured PDMS in the lamination chamber. This facilitated the removal of PDMS from the wafer upon curing. The kapton was treated using a Harrick Asher with 300mTorr of O_2 gas for 2 min at 30 W. As a result of plasma treating the kapton, the PDMS film preferentially adhered to the plasma-treated Kapton, thus maintaining its full shape when delaminating from the wafer (Figure 16e). The summary of the entire lamination process with the substrate transfer technique is illustrated in Figure 17.

34
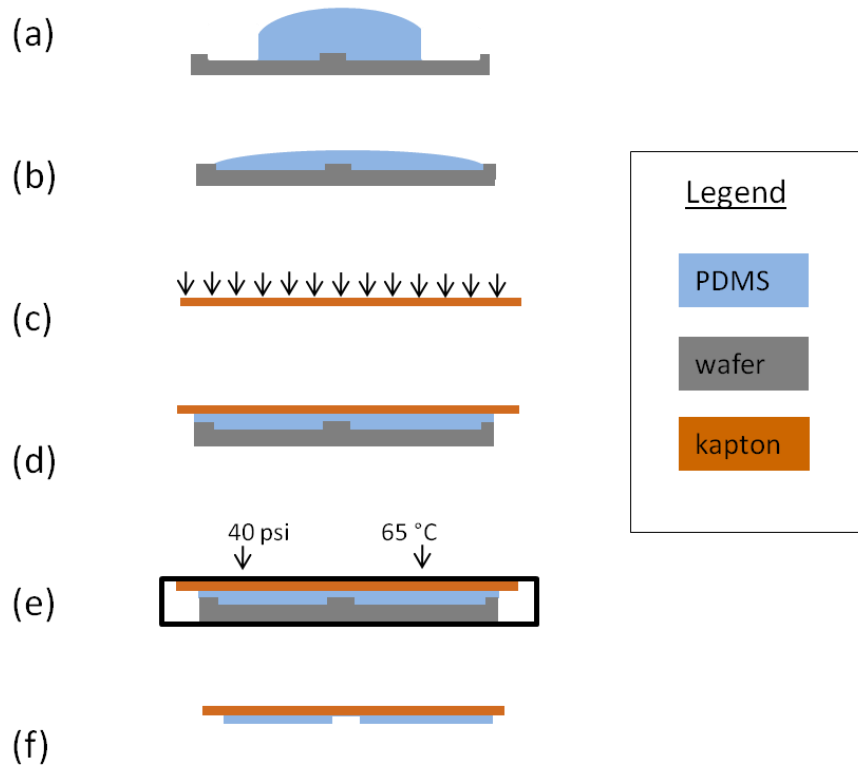
Figure 17- Lamination process used to fabricate intermediate PDMS layer
utilizing the substrate transfer technique

3.3 Device Assembly

Once all the components were fabricated and purchased, the layers were
assembled in a layer by layer process utilizing multiple bonding techniques.
Silane chemistry was used to bond the first the bottom PDMS layer to the PC
membrane in step 1, and the top PDMS layer to the opposite side of the PC
membrane in step 2 (Figure 18). Plasma bonding was utilized in assembling the
glass cover slip to the bottom PDMS layer in step 3, and fluidic ports to the top of
the PDMS layer in step 4 (Figure 19). The order of the layer by layer assembly
was important to the device fabrication protocol because to optimize bonding
conditions.

35
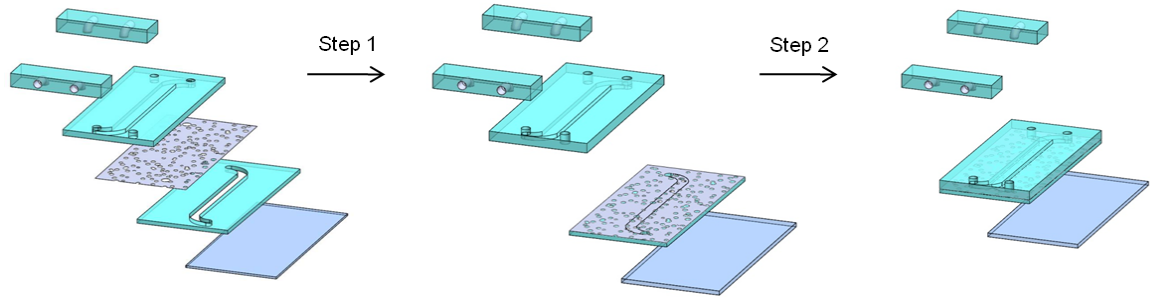
Figure 18- Bonding PC to top and bottom PDMS layers

A previously reported bonding technique utilizing silane chemistry was modified to bond the bottom PDMS layer to PC membrane using wet 3-aminopropyltriethoxysilane (APTES) chemistry[71]. The top PDMS layer was also bonded to the other side of the PC membrane using APTES chemistry; however, significant modifications were made to the previous bonding protocol (Figure 18). First, the bottom PDMS layer (still present on the kapton substrate from the lamination step) was plasma treated using a Harrick Asher with 300mTorr of O_2 gas for 2 min at 30 W. Next, the plasma treated bottom PDMS layer was submerged in a silane solution (APTES)/water (5/95%v) and heated for 20 min at 80 °C. The APTES treated bottom PDMS layer was then bonded to untreated PC membrane by placing the PC membrane on top of the bottom PDMS layer and heating for 5 min in a 37 °C oven.

In step 2, the top PDMS layer was bonded to the exposed side of the PC membrane using APTES chemistry (Figure 18). Again, significant modifications were made to the previous APTES bonding protocol. First, the top PDMS layer was plasma treated using a Harrick Asher with 300mTorr of O_2 gas for 2 min at 30 W. Next, the plasma treated top PDMS layer was submerged in a silane

36

solution (APTES)/water (5/95%v) and heated for 20 min at 80 °C. After the top PDMS layer was surface treated, it was aligned over the PC/bottom PDMS stack. The top PDMS layer was carefully lined up under an angled light source to align the intermediate PDMS channels to the top PDMS layer channels. To reduce bonding defects in the intermediate PDMS/PC membrane/top PDMS stack, a gradual curing protocol was employed: first dehydrated at room temperature for 1-3 hrs, then heated at 37 °C for 3-8 hrs and finally at 65 °C for 1-3 hrs. Fluidic ports were punched using a biopsy punch through the three layers. The kapton, still adhered to the intermediate PDMS layer, was released from the laminated PDMS layer by the spraying IPA at the adherence interface and cautiously pealing the partially bonded PDMS/PC stack off of kapton.
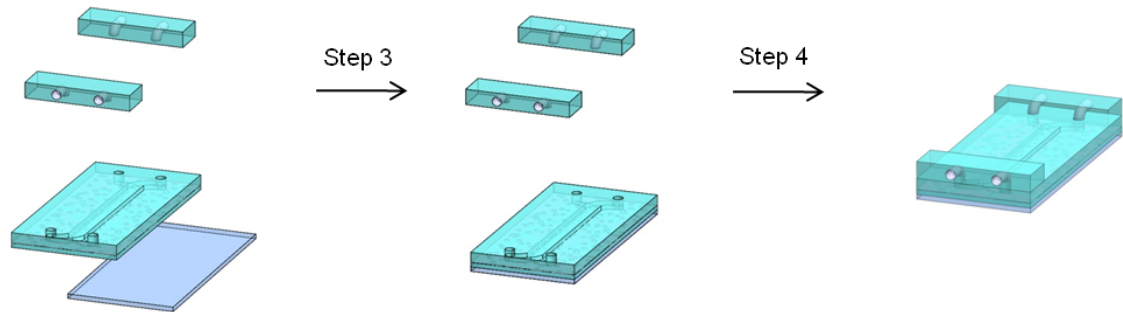
Figure 19- Plasma bonding PDMS fluidic ports and glass cover slip bottom to device

The glass cover slip and the fluidic ports were bonded using well characterized plasma bonding chemistry[69]. In plasma bonding, PDMS and glass can be bonded with or without water after both surfaces are pre-treated with O_2 plasma. Specific O_2 plasma conditions are optimized based on the specific

equipment used. First, a No. 1 glass cover slip and bottom PDMS surface of the stack were plasma treated using a Harrick Asher with 300mTorr of O_2 gas for 2 min at 30 W. The two surfaces were sprayed with DI water to aid with alignment. The stack was again cured in a gradual heating protocol: first over a 37 °C hotplate for 5 hrs, then in a 37 °C oven for 2 hours, and finished in a 65 °C oven for 2 hours. After the cover slip was bonded to the stack, the same bonding protocol was used to bond fluidic ports to the top PDMS layer surface of the stack (Figure 19). First, the fluidic ports and the top PDMS were plasma treated using a Harrick Asher with 300mTorr of O_2 gas for 2 min at 30 W. The two surfaces were sprayed with DI water to aid with alignment, and the chip ports were aligned carefully with the manifold ports. The stack was cured in a 65 °C oven for 2 hours, completing the entire device fabrication protocol.

Chapter 4

Results and Discussion

4.1 Component Fabrication

The fabrication of components and assembly of the device were all optimized successfully to tailor the device for creating an *in vitro* model of the liver malaria infection. The component fabrication, the design layout, wafer surface treatment, top layer PDMS spin conditions, and intermediate PDMS layer lamination conditions were all optimized to fit device requirements. For the device assembly, a substrate transfer technique was invented, an APTES bonding technique was modified, and the order of bonding layer was optimized.

The mask layout was modified multiple times for the bottom PDMS layer. In the original masks for the bottom PDMS layer, the outlines of the chips were dashed lines and the channel widths were 500 μm without any posts (Figure 13e). The original dashed outline was designed to aid the PDMS thin film in lifting off with kapton during removal from the laminator. Instead, the dashed lines caused tearing of laminated PDMS thin films upon removal from the wafer. Therefore, the first modification to the bottom PDMS wafer pattern was changing all the chip outlines from dashed to full lines.

The next modification to the device layout was the adjustment of the channel widths. The original design width for both the top and bottom PDMS channels was with equal 500 μm width dimensions. Aligning two 2 cm long

39

channels with 500 μm channel widths on the top PDMS layer with two 2 cm long channels with 500 μm channel widths on the bottom PDMS layer was very challenging. Alignment challenges stemmed from the difficulty in balancing micro-feature alignment with the macro scale configuration. For example, when the top and bottom channel were aligned accurately on the right end of the picture, the left end of the device alignment was shifted. To address the alignment challenges, the bottom channel width was redesigned with a 250 μm width, providing an alignment buffer of 250 μm, The reduction of the intermediate channel width improved alignment yield significantly.

Another important modification to the bottom PDMS layer mask was the addition of posts around the entire chip parameter. Uniform load distribution is required for optimum lamination conditions over the polymer covered wafer. Alignment of the chamber piston over the wafer chip was improved with the addition of the posts, and thus the load distributed more evenly. In result, yield of successfully laminated intermediate PDMS layers was increased from 0% to 77% because the posts improved pressure uniformity and displacement within the lamination chamber.

The wafer surface treatment to prevent PDMS from sticking to the mold was optimized next. Triethoxysilane and trichlorosilanes were each tested under 3 different conditions (no heat, 10 min at 110 °C, and 30 min at 110 °C) for the best wafer non-sticky surface treatment, shown in Table 1. All 6 surface treatment protocols were tested for how much residue of PDMS was left on the wafer upon removal of PDMS. If the PDMS was lifted off the wafer without any

40

tears, then a check was marked to indicate a successful surface treatment. If PDMS residue was left over on the wafer, then the trial failed and was marked as an "x." Without any surface treatment, the PDMS residue got stuck to the wafer after the first attempt. Wafers treated with triethoxysilane without heat showed some PDMS residue on the wafers upon lift off. With both 10 min and 30 min of 110 °C heat after the triethoxysilane treatment, wafers exhibited inconsistent results. Trichlorosilane exhibited almost perfect protection without heat and perfect protection when heated at 110 °C. Therefore, vapor deposited trichlorosilane with heat activation at 110 °C for 10 min was chosen as the optimal surface treatment condition for every wafer fabricated for this device.

Table 1- Optimization of the wafer surface treatment results indicating successfully pealed PDMS from wafer or partially adhered PDMS

PDMS Peel #	1	2	3	4	5	6	7	8	9	10	11	12	13	14
Control:	x	x	x	x	x	x	–	–	–	–	–	–	–	–
No Silane	x	x	x	x	x	x	–	–	–	–	–	–	–	–

Triethoxy Silane

	1	2	3	4	5	6	7	8	9	10	11	12	13	14
No Heat	x	x	x	x	x	x	–	–	–	–	–	–	–	–
	x	x	x	x	x	x	–	–	–	–	–	–	–	–
10 min at 110C	x	✓	x	x	✓	✓	✓	x	✓	✓	x	✓	✓	✓
	✓	✓	✓	✓	x	✓	✓	✓	x	✓	✓	✓	✓	✓
	x	✓	x	x	x	x	x	x	x	✓	✓	✓	✓	✓
30 min at 110C	✓	✓	x	x	✓	✓	x	✓	✓	✓	✓	✓	✓	✓

Trichloro Silane

	1	2	3	4	5	6	7	8	9	10	11	12	13	14
No heat	✓	✓	✓	✓	✓	✓	✓	✓	✓	✓	✓	✓	✓	✓
	x	✓	✓	✓	✓	✓	✓	✓	✓	✓	✓	✓	✓	✓
	✓	✓	✓	✓	✓	✓	✓	✓	✓	✓	✓	✓	✓	✓
10 min at 110C	✓	✓	✓	✓	✓	✓	✓	✓	✓	✓	✓	✓	✓	✓
	✓	✓	✓	✓	✓	✓	✓	✓	✓	✓	✓	✓	✓	✓
	✓	✓	✓	✓	✓	✓	✓	✓	✓	✓	✓	✓	✓	✓
30 min at 110C	✓	✓	✓	✓	✓	✓	✓	✓	✓	✓	✓	✓	✓	✓

41
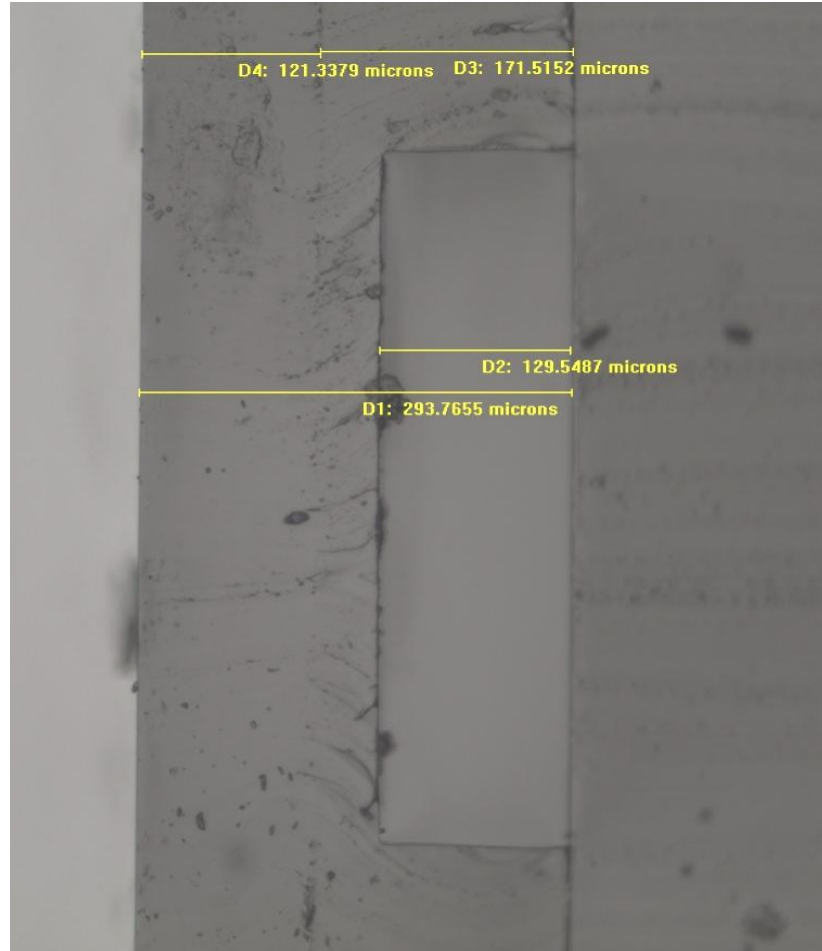
Figure 20- Spun PDMS bonded to another PDMS block and cut at a 90 ° angle for thickness measurement under a microscope

The PDMS spin protocol was optimized for fabricating a 230 μm top PDMS layer. First, a spin curve of spin speed versus resulting PDMS thickness was created as a starting point. PDMS thickness was measured by bonding the spin layer to another PDMS block, cutting the stack at a 90 ° angle and measuring under a calibrated microscope. Figure 20 shows an example of spun PDMS thickness measurement images. While PDMS thickness close to 230 μm could be achieved with one spin, thickness varied largely by over 20% over the

42

entire wafer area. Therefore, the PDMS was fabricated in 2 spin layers to a total of 230 μm thickness. To promote even distribution of the PDMS, the uncured polymer was spread on the wafer for 1 min before the spinning was started. After the wafer was spun at 650 RPM for 60 seconds, it sat undisturbed for 5 minutes to allow the excess PDMS on the wafer edges to even out prior to moving to the oven. The combination of 2 layer spin protocol and addition of wait time before and after spinning the polymer resulted in a reproducible yield of a 230 μm PDMS film for the top device layer.

Multiple lamination conditions were modified to fabricated the bottom PDMS layer with a fully punched through pattern. First, the pressure in the chamber was increased from 20psi to 40 psi from the original protocol[70]. Excess of uncured PDMS results in PDMS residue left over in the channels, yet scarcity of PDMS causes a lot of bubbles to be formed in the cured polymer when depositing kapton. PDMS was poured on a wafer mold on a mass balance and after numerous weights were tested, an optimal 1.8 g of PDMS was determined based on observing the least PDMS residue with enough PDMS for even cushion for the kapton deposition. While the 1.8 g of PDMS was optimal for preventing bubbles, the layers were still laminated with PDMS residue in the channels. To avoid the residue formation, the wafer mold with 1.8 g of PDMS was placed on the spinner and rotated at 600RPM for 45 seconds to even out the polymer distribution prior to lamination. Finally, with the increased pressure, optimized PDMS weight, and the spinning step added, the intermediate PDMS layer laminated without PDMS residues in the channels.

43
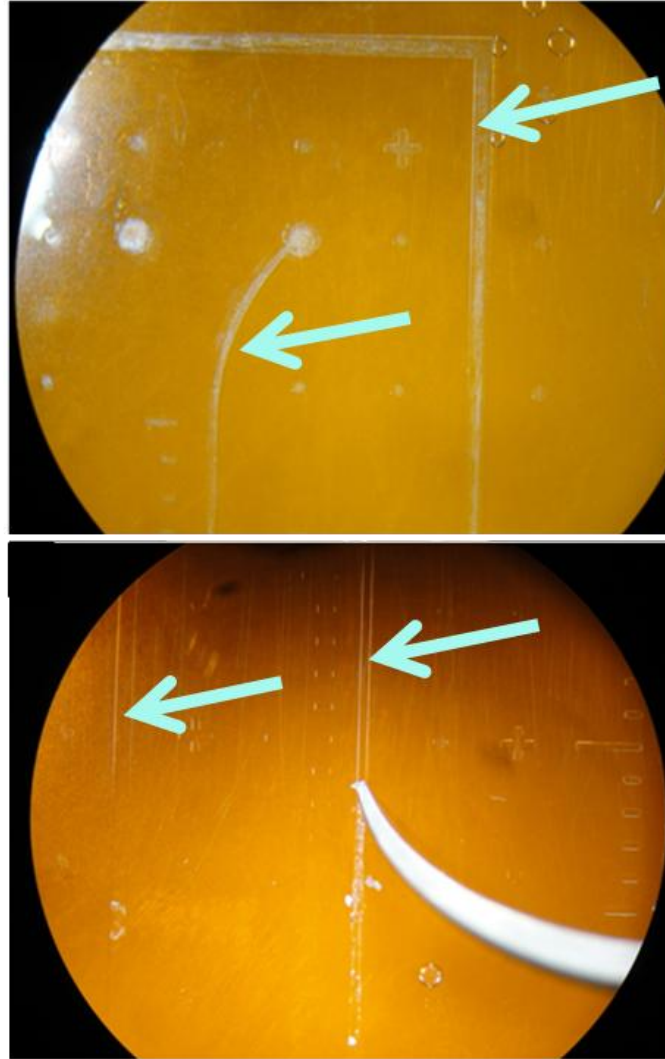
Figure 21- Analysis of lamination process results

Laminated PDMS filmed were examined under a microscope during optimization testing because a significant portion of the laminated layers did not yield PDMS with entirely punched through channels. PDMS residue was always observed in the channels, but completely punched through films only had trace amounts of residue in the channels. The trace PDMS residue appeared "cloudy" under magnification (Figure 23). Therefore, films with "cloudy" channels were

44

marked as successful laminations. PDMS films which failed to laminate through resulted with excess PDMS in the channels and clear channel areas were observed (Figure 23).

4.2 Substrate Transfer Technique and Device Assembly

A previously reported method is similar to the substrate transfer technique that was utilized in the fabrication of this microfluidic chip[71]. Briefly, Zhang *et al.* reported a method to temporary bond PDMS to a carrier substrate also made of PDMS for the transfer of thin non-free standing PDMS films from one substrate to another; thus, enabling otherwise not achievable complex polymer three dimensional geometries[71]. Unlike the previous method, which employed the use of PDMS as the carrier material, the technique invented for this device employed kapton as a carrier material for the transfer of the thin PDMS layer to another substrate without creating any feature distortion that is often observed as the PDMS stretches.

Kapton has multiple advantages as a carrier material over PDMS. First, kapton allowed for a clear interface distinction between the carrier material and patterned PDMS as opposed to using PDMS as the carrier material for PDMS. In addition, as a tough, high temperature thermoplastic, kapton can withstand high mechanical loads useful for creating punched through patterned PDMS molds. Both techniques offer the potential to create three dimensional PDMS patterns with a layer by layer process. This opens up the ability to create complex geometric features for applications beyond *in vitro* models. On the whole, kapton

45

provided transparency and flexibility for feature alignment and the strength to endure high temperatures and pressures for molding and then transferring PDMS for a layer by layer assembly.
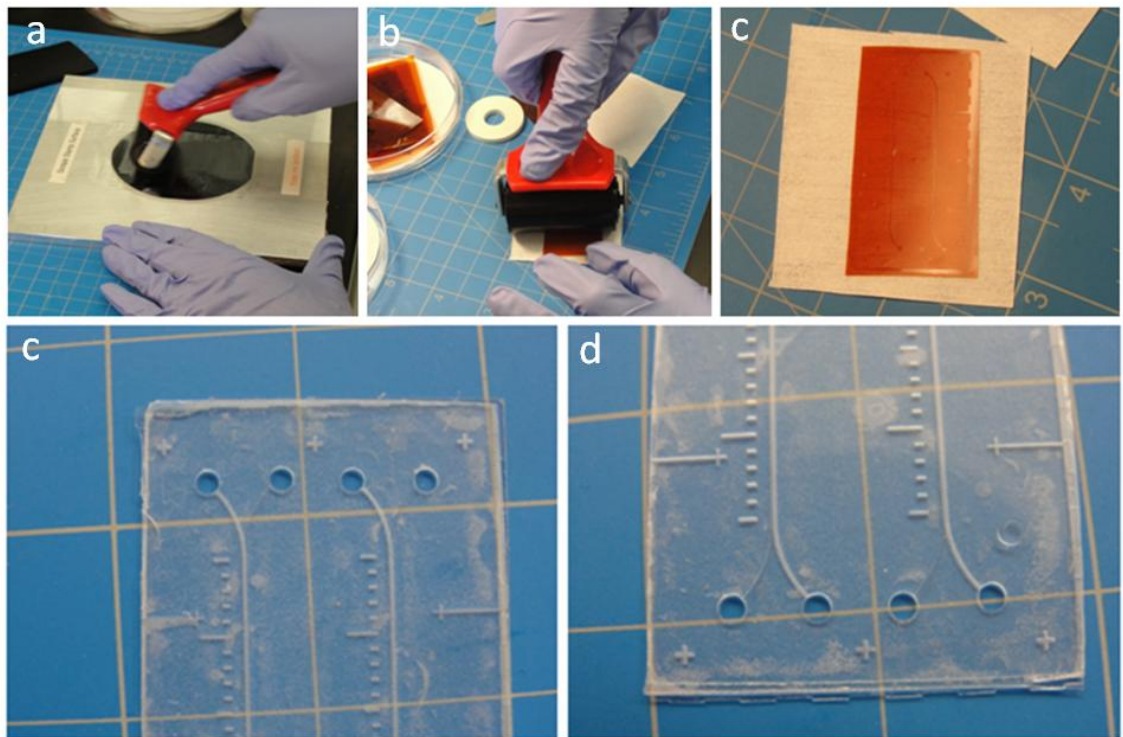
Figure 22- Bonding device layers with a Si adhesive

Following successful substrate transfer development, the device components had to be assembled and bonded via a layer by layer process. First, adhesive methods were considered. Silicone based polymer adhesives are the most conventional for bonding PDMS to PC. Specifically fo this study, the Dow Corning 3140 biocompatible silicone based adhesive was considered. A roll on method was utilized to deposit a uniform thin adhesive layer by rolling the adhesive onto the roller and then rolling the adhesive onto the PDMS layer

46

(Figure 22a-b). This technique, however, resulted in imperfections over the entire area of the polymer because the surface defects built up over the addition of 6 layers of materials (Figure 22c-d). Therefore, other methods were explored for bonding PC to PDMS.

A solvent based APTES chemistry method was utilized to sandwich the PC membrane between the top layer and the intermediate PDMS layers[71]. Aran *et al.* reported that oxygen plasma treating PC and PDMS surfaces followed by a wet APTES treatment of the PC, resulted in an irreversible bond when heated. However, we found that when attempting to bond a second PDMS layer to a PC/PDMS stack, the bond between the stack was broken upon plasma treating the exposed PC material of the stack. Therefore, the first modification to this technique was to pre-treat both sides of the PC membrane (with oxygen plasma) before bonding either side to PDMS.

The reversal of the silane chemistry from PC to PDMS was observed to still yield a strong bond. The originally proposed APTES bonding method suggested that plasma treating PC and PDMS with oxygen plasma, followed by the silane treatment of the PC, would result in a PC and PDMS irreversible bond upon heating[71]. However, it was also discovered that that plasma treating PC and PDMS with oxygen plasma, followed by the silane treatment of the PDMS, would result in a PC and PDMS irreversible bond upon heating. Reversing silane chemistry surface treatment from PC to PDMS was an important modification, because the PC membrane did not need to be suspended in a wet APTES

47

solution. A dry PC membrane retained its structural integrity during the assembly process.

The APTES bonding method also had to be modified to address bonding quality between PDMS and PC. Bubbles and bonding imperfections were observed during device development (Figure 23). To eliminate bubbles and uneven bonding, the APTES bonding protocol was modified from a single temperature cure to multiple incremental heating steps. This reduced bonding defects, such as bubbles, between the membrane and PDMS interface. Figure 23 shows the improved bonding quality in the bottom device.
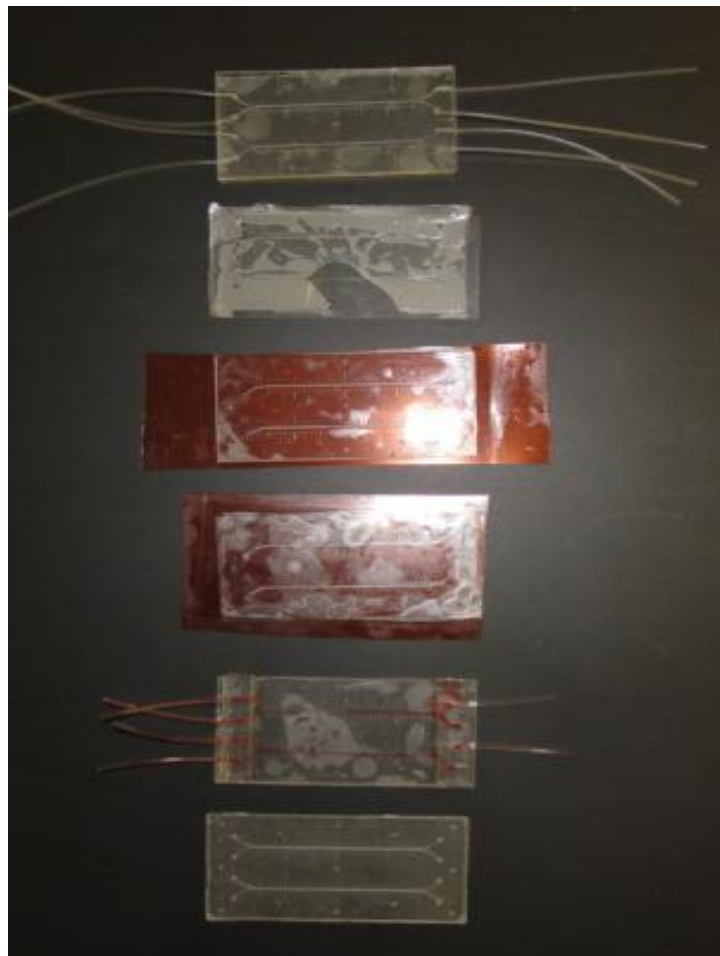
Figure 23- Examples of experiment with failed bonding protocols and a bubble free final device at the bottom

48

4.3 Final Device

Microfluidic chips were successfully fabricated to meet all the design criteria for studying *in vitro* malaria parasite infection (Figure 24). The device included a membrane integrated design to mimic the architecture of a liver, cell chamber dimensions affable for high-resolution imaging, and fluidic port design for optical access to both sides of the membrane. The goals were met by deliberate design planning, component fabrication, assembly optimization, and the invention of a substrate transfer technique.
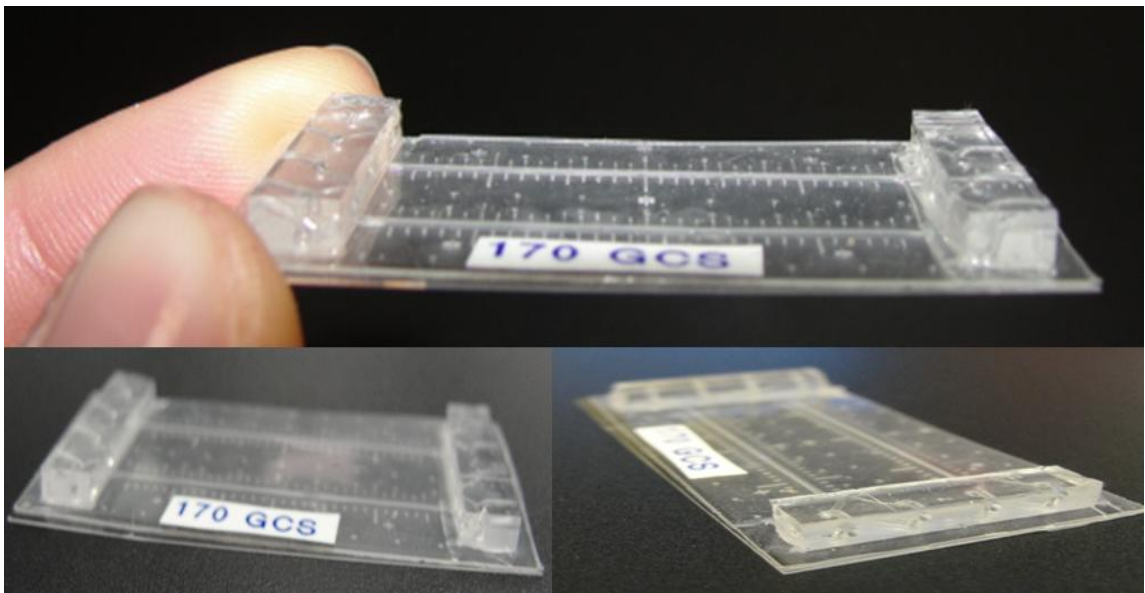
Figure 24- Fully fabricated chip with 2 devices and fluid ports

In addition to successfully fabricating the multiplexed chip, a holder was custom built to fit into a microscope frame and stage. Figure 25 shows an image of the chip enclosed in the rapid prototyped holder and the holder and chip assembly mounted in a standard microscope frame. The holder design allows

49

for the chip and holder assembly to be flipped upside down enabling optical access to both sides of the membrane without removing the fluidic tubing. The low profile fluidic port design of the manifold on the chip and the low profile of the holder were designed to accommodate for the lateral movement of the objectives in the goal of achieving a high-resolution imaging system for live cell culture. The entire system of the device chip and custom holder sitting in the frame of the microscope are seen in Figure 26.
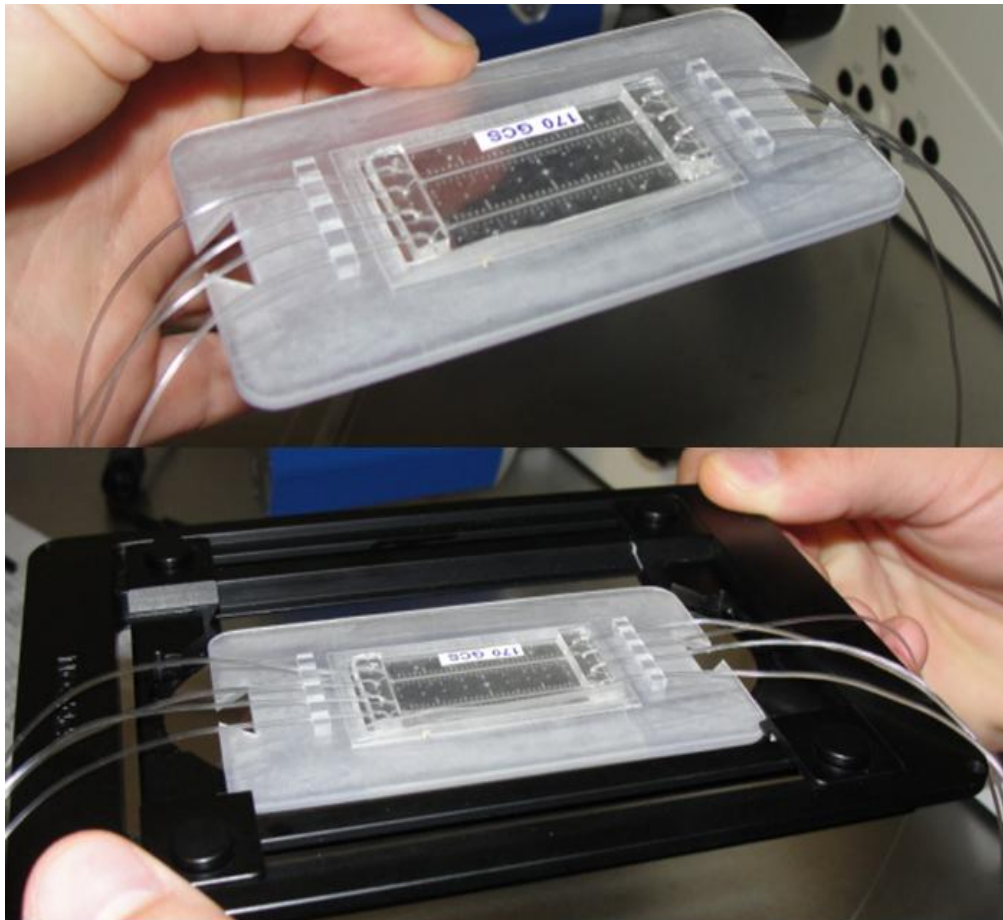
Figure 25- Chip enclosed in a custom holder on top and the entire assemble fit into a standard Leica microscope frame
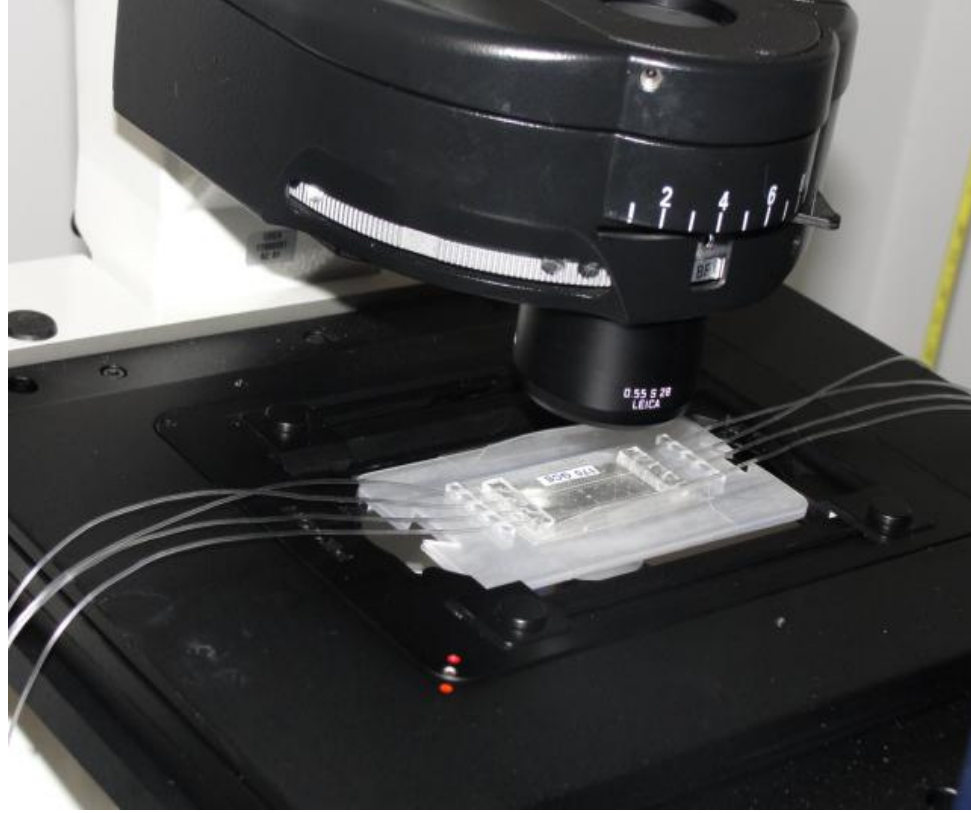
Figure 26- Final chip enclosed in a custom built holder fit in a standard Leica frame on the Leica microscope stage

Shear stress calculations were performed to determine flow rates in the chip that would mimic true *in vivo* liver conditions and to check the device bonding robustness at the desired flow rates. The critical physiological parameter to control with flow rate is the shear stress induced by the flowing media on the surface of the cells. In order to estimate the potential shear stress that the cells attached to the surface will experience, the Navier-Stokes equation (1) was derived for flow between parallel plates where T was shear stress [dynes/cm^2], Q was flow rate [mL/hr], b was chamber slit width [cm], h was channel height [cm] and μ was the viscosity [dynes*s/cm^2]. The channel height

51

for both the top and bottom chambers was 0.01 cm and the viscosity of the fluid was 0.01 dynes*s/cm^2 as cell media is mostly composed of water.

$$T = \frac{6Q\mu}{bh^2}$$ (1)

Literature suggested that endothelial cells of a liver sinusoid experience shear stress between 10-15 dynes*s/cm^2 as blood flows over them[22-23], while hepatocytes, shielded by the space of Disse from the direct flow (see Figure 2), experience minimal shear stress[24-25]. It has been shown that hepatocytes function more naturally at lower shear stresses of between 0.01-.033 dynes*s/cm^2, and this suggests a target upper limit for the shear stress experienced by the hepatocytes of 0.033 dynes*s/cm^2.
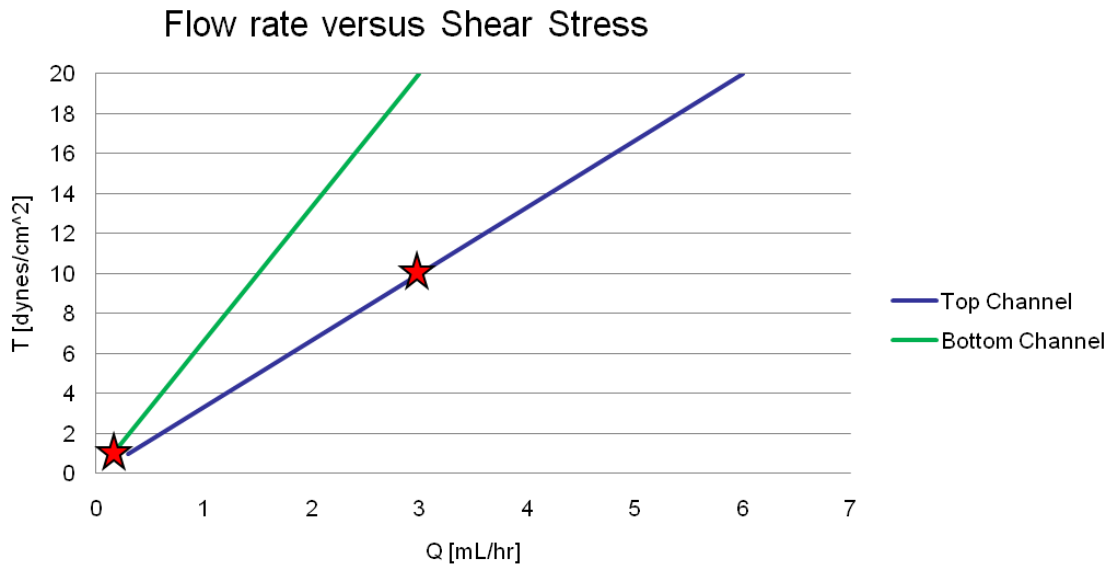
Figure 27- Flow rate versus shear stress to determine the optimum flow conditions for hepatocyte chamber

52

Flow rate versus shear stress was graphed for both the top and bottom channels in the hepatocyte culture and the endothelial culture cases (Figure 27). Here it is shown that in order not to exceed the recommended hepatocyte shear stress, the flow rate in the hepatocyte chamber should be lower than 36 µL/hr. A physiologically relevant flow range for the endothelial side was calculated to 3 mL/hr. To test for the integrity of the device bonding, flow rates of up to 20 mL/hr were tested and did not rupture the bonds, providing a range of flow that allowed for the flow-induced shear stress range desired. Therefore, the designed and fabricated channel dimensions allow for conditions mimetic of the shear stress micro-environment in the liver sinusoid.
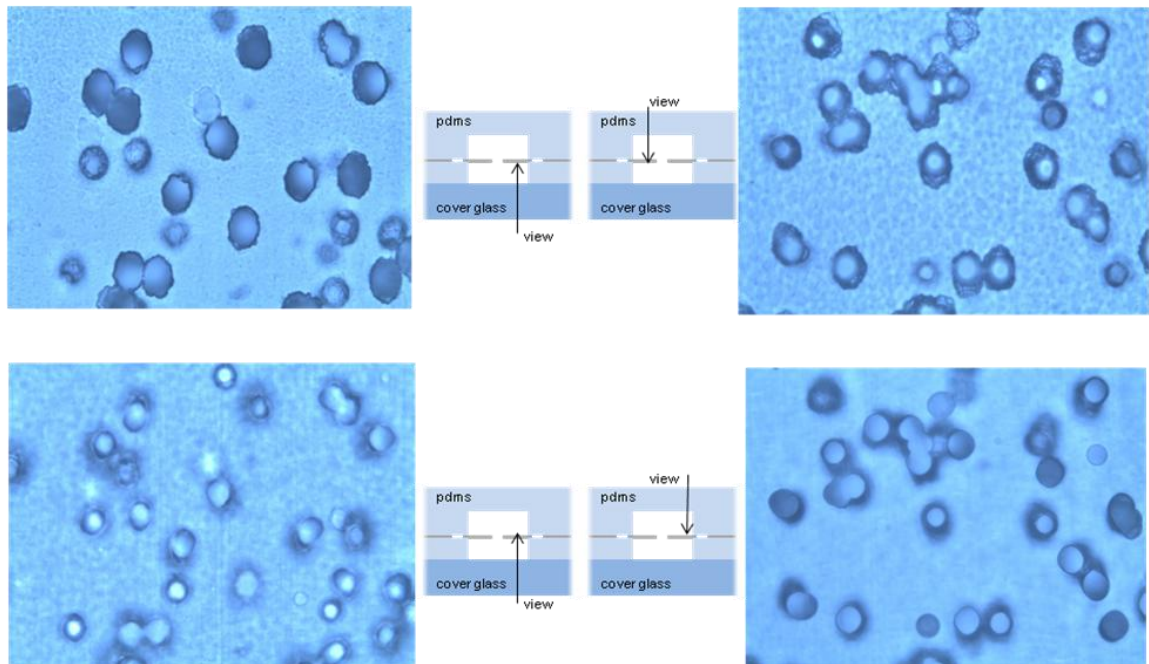
Figure 28- Oil immersion 63X images of the PC membrane through device showing high resolution imaging access from both sides of the device

The PC membrane was imaged through the device chamber to demonstrate optical access to both sides of the membrane. Because of the manufacturer's fabrication process for making 10 μm pores in a PC membrane, the material has a rough and a smooth side. For consistency, all devices were fabricated with the rough side of the PC membrane facing the glass cover slip and the smooth side of the membrane facing the top PDMS material. Figure 28 shows the rough and smooth sides of PC membrane imaged from both the glass coverslip side and the PDMS side of the membrane. The rough side of the membrane is imaged through the glass coverslip directly and through the PDMS membrane. Although the roughness is seen more clearly from the glass coverslip, it is important to note that the rough side of the membrane can still be accessed optically through the membrane. Furthermore, the images demonstrate successful imaging with high-resolution imaging as the images were taken with an oil immersion, 63X objective on a Leica microscope.

To further demonstrate high-resolution capability of the device, live cell culture images capturing otherwise hidden sub-cellular components were provided by courtesy of Steven Maher as a proof of concept (Figure 29). To obtain the images, a human hepatoma line HepG2 (ATCC) was maintained on collagen I coated plates in manufacturer's recommended media supplemented with bovine serum albumin. After seeding the cells into the device, the opposing chamber was perfused during subsequent culture, live-cell staining and imaging.
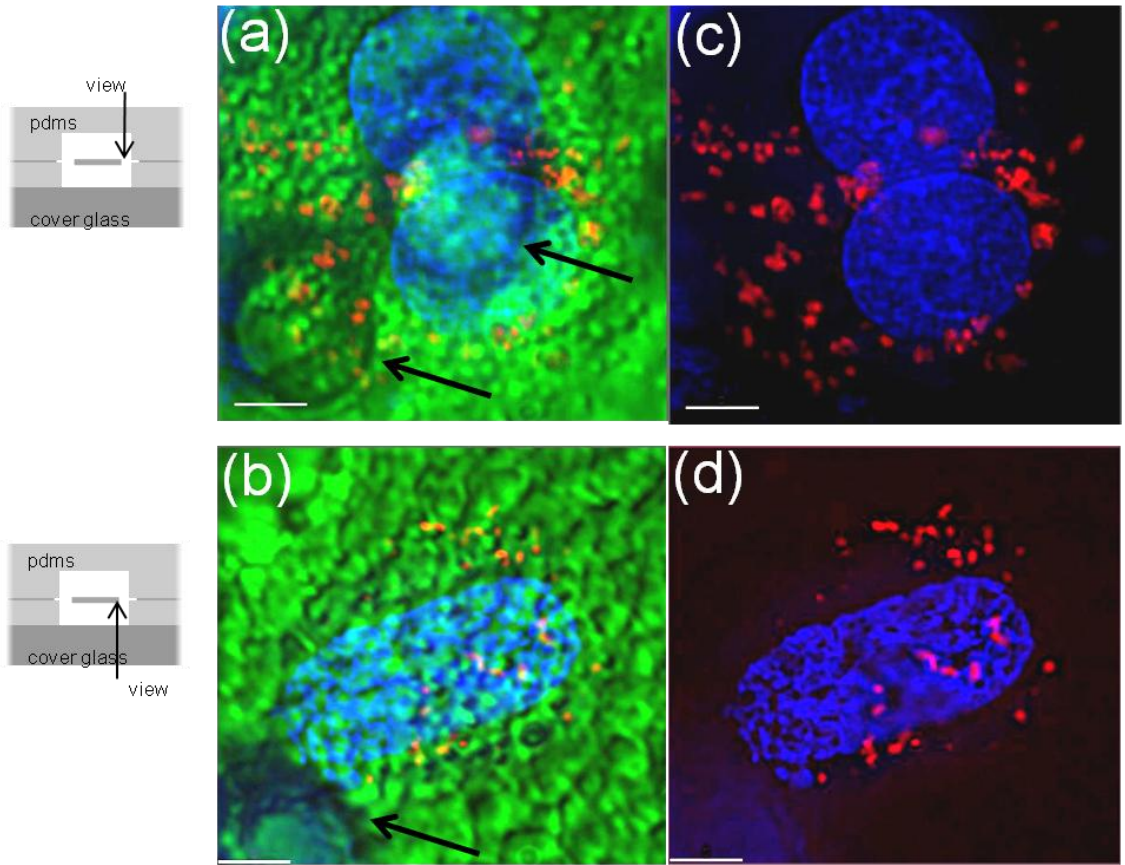
Figure 29- High Resolution live cell imaging of hepatocytes

The sub-cellular clarity of the images in the figure taken with a 100x oil immersion objective (Olympus), and subsequent software deconvolution (DeltaVision), is impressive and is uniquely enabled by the careful control of the device layer thickness. Bright view images (Figure 29a and Figure 29c) and fluorescent images of live cell culture (Figure 29b and Figure 29d) were taken on one side of the membrane from the top view of the device. In addition, live cell culture on the opposite side of membrane was captured through the glass cover slip bottom view (Figure 29c and Figure 29d). Hoescht stain was used to stain the nuclei blue and Mitotracker stain was used to stain the mitochondria red.

55

The ability to visualize subcellular components of live cell culture proved that the device design succeeded for use in optical high-resolution microscopy by accounting for working distance limitations with thin dimentions. In addition, the image was taken under continuous perfusion without interrupting cell culture development. Finally, cell culture on both sides of the membrane was opticially accessed with high resolution microscopy, assuring successful implementation low fluidic port design. The high resolution imaging capability to capture sub-cellular components on both sides of the membrane in live cell culture is a distinct novelty of this microfluidic device that will enable studies to potentially discover malaria therapeutics.

56

Chapter 5

Conclusions

In conclusion, a membrane-integrated microfluidic research device for studying liver stage malaria development was successfully designed and fabricated. By fabricating cell chambers for selective cell seeding on both sides of a membrane, the liver sinusoid architecture, important for the biology of the parasite infection, can be mimicked. The cell environment in each chamber can be tuned to exhibit *in vivo* cell specific shear stress conditions of 10-15 dynes*s/cm^2 in one chamber and 0.01-0.33 dynes*s/cm^2 in the second cell chamber. The microfluidic device design allows for continuous perfusion of nutrients. Furthermore, fluid port design features enable optical access to both sides of the membrane. To account for working distance limitations of high-resolution optical microscopy, the device thickness was minimized to a total 230 μm height beyond each side of the membrane. This device fulfilled all requirements to advance research of an *in vitro* model of the liver stage malaria by mimicking cell architecture and shear stress conditions, enabling flow perfusion, and allowing for high-resolution optical imaging of live cell culture on both sides of the membrane.

Applications for the device reach beyond its use as an *in vitro* model of the liver stage malaria parasite. Because the device was designed as an *in vitro* liver model, other liver disease developmental studies can be performed. Additional

57

applications for the device beyond use as a liver model include innovative studies in various multilayer tissue models, trans-membrane transport phenomena, and observation of sub-cellular processes and components in such systems. Furthermore, because of the high-resolution optical access to both sides of the membrane, this device could be used in high content screening applications in drug development.

The novel substrate transfer technique developed for device fabrication is a useful tool beyond this application. The development of the thin PDMS transfer technique using kapton as a carrier material enables the facile construction of complex 3D geometries fabricated via layer by layer process. The substrate transfer technique generates minimal feature distortion during the movement of a thin polymer film from one substrate to another.

Future advancements in this platform may include membrane development, expanding the high throughput (multiplexed) design, and further vertical and horizontal compartmentalization of the model through additional chambers or surface patterning. These advancements would enable further defined cellular constructs, providing the means to improve physiologically relevant *in vitro* models with observation capabilities suited for high throughput drug discovery and basic biological research. In addition, the fabrication techniques used can be refined and developed for faster and more automated manufacturing techniques.

58

References

1   W. Snow, C. A. Guerra, A.M. Noor, H.Y. Myint, H.Y. Hla, S.I. Hay. The global distribution of clinical episodes of Plasmodium falciparum malaria. *Nature*, 2005, 434: 214-217

2   A. Sturm, R. Amino, C. van de Sand, T. Regen, S. Retzlaff, A. Rennenberg, A. Krueger, J.M. Pollock, R. Menard, V.T. Heussler. Manipulation of host hepatocytes by the malaria parasite for delivery into liver sinusoids. *Science*, 2006, 313: 1287-1490

3   J. Sattabogkot, N. Y. Ychoke, S. Leelaudomlipi, M. Rasameesoraj, R. Jenwithisuk, R.E. Coleman, R. Udomsangpetch, L. Cui, and T.G. Brewer. Establishment of a human hepatocyte line that supports in vitro development of the exo-erythrocytic stages of the malaria parasites *Plasmodium falciparum* and *P. vivax*. *American Journal of Tropical Medicine and Hygiene*, 2006, 74: 708-715

4   L.K. Basco, J. Bickii, P. Ringwald. *In-vitro* activity of primaquine against the asexual blood stages of *Plasmodium falciparum. Annals of Tropical Medicine and Parasitology*, 1999, 93: 179-182.

5   N. Vale, R. Moreira, P. Gomes. Primaquine revisited six decades after its discovery. *European Journal of Medicinal Chemistry*, 2009, 44: 937-953

6   D. Mazier, R. L. Beaudoin, S. Mellouk, P. Druilhe, B. Texier, J. Trosper, F. Miltgen, I. Landau, C. Paul, O. Brandicourt, C. Guguen-Guillouzo, P. Langlois. Complete Development of Hepatic Stages of Plasmodium falciparum *in vitro. Science,* 1985, 227: 440-442

7   A. Gego, O. Silvie, J.F. Franetich, K. Farhati, L. Hannoun, A.J. Luty, R.W. Sauerwein, C. Boucheix, E. Rubinstein, D. Mazier. New approach for high-throughput screening of drug activity on Plasmodium liver stages. *Antimicrobial Agents* and *Chemotherapy*, 2006, 50: 1586-1589

8   G.M. Walker, H.C. Zeringue, D.J. Beebe. Microenvironment design considerations for cellular scale studies. *Miniaturization for Chemistry, Biology and Bioengineering,* 2004, 2: 91-97

9   S.N. Bhatia, U.J. Balis, M.L. Yarmush, M. Toner. Effect of cell-cell
    interactions in preservation of cellular phenotype: cocultivation of
    hepatocytes and nonparenchymal cells. *The Federation of American
    Societies for Experimental Biology Journal*, 1999, 13: 1883-1900

10 S.N. Bhatia, M.L. Yarmush, M. Toner. Controlling cell interactions by
    micropatterning in co-cultures: hepatocytes and 3T3 fibroblasts. *Journal of
    Biomedical Materials Research,* 1997, 34:189-199

11 P. Krause, F. Saghatolislam, S. Koenig, K. Unthan-Fechner, I. Probst.
    Maintaining hepatocyte differentiation in vitro through co-culture with
    hepatic stellate cells. *In Vitro Cellular* & Developmental *Biology - Animal*,
    2009, 45 :205-212

12 S.R. Khetani, S.N. Bhatia. Microscale culture of human liver cells for drug
    development. *Nature Biotechnology*, 2008, 26: 120-126

13 H. Otsuka, A. Hirano, Y. Nagasaki, T. Okano, Y. Horiike, and K. Kataoka.
    Two-dimensional multiarray formation of hepatocyte spheroids on a
    microfabricated PEG-brush surface. *ChemBioChem*, 2004, 5:850-855.

14 T. Tamura, Y. Sakai, and K. Nakazawa. Two-dimensional microarray of
    HepG2 spheroids using collagen/polyethylene glycol micropatterned chip.
    Journal of Material Science: Materials in Medicine, 2008, 19: 2071-2077.

15 S. March, E.E. Hui, G. H. Underhill, S.Khetani, S.N. Bhatia.
    Microenvironmental regulation of the sinusoidal endothelial cell phenotype
    in vitro. Hepatology, 2009, 50: 920–928

16 C. H. Cho, J. Park, A. W. Tilles, F. Berthiaume, M.Toner, M. L. Yarmush.
    Layered patterning of hepatocytes in co-culture systems using
    microfabricated stencils. *BioTechniques*, 2010, 48: 47-52

17 B.J. Kane, M.J. Zinner, M.L. Yarmush, M. Toner. Liver-Specific Functional
    Studies in a Microfluidic Array of Primary Mammalian Hepatocytes.
    Analytical Chemistry, 2006, 78: 4291–4298.

18 A. Carraro, W.M. Hsu, K.M. Kulig, W.S. Cheung, M.L. Miller,
    E.J. Weinberg, E.F. Swart, M. Kaazempur-Mofrad, J.T. Borenstein,
    J.P. Vacanti and C. Neville. *In vitro* analysis of a hepatic device with
    intrinsic microvascular-based channels. *Biomedical Microdevices*, 2008,
    10: 1387-2176

19 S. Ostrovidov, J. Jiang, Y. Sakai, T. Fujii. Membrane-Based PDMS
    Microbioreactor for Perfused 3D Primary Rat Hepatocyte Cultures.
    Biomedical Microdevices, 2004, 6: 279-287

60

20 J.F. Borenstein, E.J. Weinberg, B.K. Orrick, C. Sundback, M.R. Kaazempur-Mofrad, J.P. Vacanti. Microfabrication of Three-Dimensional Engineered Scaffolds. *Tissue Engineering*, 2007, 13: 1837-1844

21 M. Shin, K. Matsuda, O. Ishii, H. Terai, M. Kaazempur-Mofrad, J. Borenstein, M. Detmar, J.P. Vacanti. Endothelialized Networks with a Vascular Geometry in Microfabricated Poly(dimethyl siloxane). *Biomedical Microdevices,* 2004, 6: 269-278

22 H. Nakatsuka, T. Sokabe, K. Yamamoto, Y. Sato, K. Hatakeyama, A. Kamiya, J. Ando. Shear stress induces hepatocyte PAI-1 gene expression through cooperative Sp1/Ets-1 activation of transcription. *American Journal of Gastrointestinal* and *Liver Physiology,* 2006, 291: G26-G34

23 A.W. Tilles, H. Baskaran, P. Roy, M.L. Yarmush, M. Toner. Effects of Oxygenation and Flow on the Viability and Function of Rat Hepatocytes Cocultured in a Microchannel Flat-Plate Bioreactor. *Biotechnology and Bioengineering*, 2001, 73: 379-389

24 V. Shah, F.G. Haddad, G. Garcia-Cardena, J.A. Frangos, A. Mennone, R.J. Groszmann, and W.C. Sessa. Liver sinusoidal endothelial cells are responsible for nitric oxide modulation of resistance in the hepatic sinusoids. *The Journal of Clinical Investigation*, 1997, 100: 2923–2930

25 F. Braet, M. Shleper, M. Paizi, S. Brodsky, N. Kopeiko, N. Resnick and G. Spira. Liver sinusoidal endothelial cell modulation upon resection and shear stress *in vitro*. *Comparative Hepatology,* 2004, 3: 7

26 I. Meyvantsson, D. J. Beebe. Cell culture models in microfluidic systems. *Analytical Chemistry Review,* 2008. 1:423–49

27 E.J. Suuronen, H. Sheardown, K.D. Newman, C.R. McLaughlin, M. Griffith. Building in vitro models of organs. *International Review of Cytology*. 2005: 244, 137-173

28 L.G. Griffith, M.A. Swartz. Capturing complex 3D tissue physiology *in vitro*. *Nature Molecular Cell Biology*, 2006. 7: 211-224

29 L. Kim, Y.C. Toh, J.V. Voldman, H.Yu. A practical guide to microfluidic perfusion culture of adherent mammalian cells. *Lab on a Chip*, 2007, 7: 681 – 694

30 K.N. Chua, W.S. Lim, P. Zhang, H. Lu, J. Wen, S. Ramakrishna, K.W. Leong, and H.Q. Mao. Stable immobilization of rat hepatocyte spheroids on galactosylated nanofiber scaffold. *Biomaterials*, 2005, 26:25 37-2547

61

31 H. Otsuka, A. Hirano, Y. Nagasaki, T. Okano, Y. Horiike, and K. Kataoka. Two-dimensional multiarray formation of hepatocyte spheroids on a microfabricated PEG-brush surface. *ChemBioChem.* 2004. 5:850-855

32 K. R. King, C.C.J. Wang, M. R. Kaazempur-Mofrad, J. P. Vacanti, J. T. Borenstein. Biodegradable Microfluidics. *Advanced Materials,* 2004, 16: 2001-2012

33 M. W. Tibbitt, K.S. Anseth. Hydrogels as extracellular matrix mimics for 3D cell culture. *Biotechnology and Bioengineering,* 2009. 103: 655-663

34 D.M. Bissell, D.M. Arenson, J.J. Maher, and F.J. Roll. Support of cultured hepatocytes by a laminin-rich gel. Evidence for a functionally significant subendothelial matrix in normal rat liver. *Journal of Clinical Investigation*, 1987. 79:801-812

35 Y.S. Torisawa, A. Takagi, Y. Nashimoto, T. Yasukawa, H. Shiku, and T. Matsue. A multicellular spheroid array to realize spheroid formation, culture, and viability assay on a chip. *Biomaterials*, 2007. 28: 559-566

36 G.B. Salieb-Beugelaar, G. Simone, A. Arora, A. Philippi, A. Manz. Latest Developments in Microfluidic Cell Biology and Analysis Systems. *Analytical Chemistry,* 2010, 82: 4848-4864

37 M.H. Wu, S.B. Huang, G.B. Lee. Microfluidic cell culture systems for drug research. *Lab on chip*, 2010. 10: 939-956

38 H. Andersson, A. van den Berg. Microfluidic devices for cellomics: a review. *Sensors and Actuators B: Chemical*, 92: 315-325

39 J.C. Lötters, W. Olthuis, P.H. Veltink, P. Bergveld. The mechanical properties of the rubber elastic polymerpolydimethylsiloxane for sensor applications. *Jornal of Micromechics and Microengineering*,1997, 7: 145-147

40 A. Kumar, H.A. Biebuyck, G.M. Whitesides. Patterning self-assembled monolayers- Applications in Materials Science. *Langmuir*, 1994. 10: 1498-1511

41 J E.W.K. Young, D.J. Beebe. Fundamentals of Microfluidic Cell Culture in Controlled Microenvironments. *Chemical Society Reviews,* 2010, 39: 1036-1048

42 J. El-Ali, P.K. Sorger, K.F. Jensen. Cells on Chips. *Nature*, 2006, 442: 403-411

43 M.J. Powers, K. Domansky, M.R. Kaazempur-Mofrad, A. Kalezi, A. Capitano, A. Upadhyaya, P. Kurzawski, K. E. Wack, D.B. Stolz, R. Kamm, L.G. Griffith. A Microfabricated Array Bioreactor for Perfused 3D Liver Culture. *Biotechnology and Bioengineering*, 2002, 78: 257-269

44 M.T. Lam, Y.C. Huang, R.K. Birla, S. Takayama. Microfeature Guided Skeletal Muscle Tissue Engineering for Highly Organized 3-dimensional Free-standing Constructs. *Biomaterials*, 2009, 30: 1150-1155

45 J.W. Park, B. Vahidi, A.M. Taylor, S.W. Rhee, N.L. Jeon. Microfluidic Culture Platform for Neuroscience Research. *Nature Protocols*, 2006, 1: 2128- 2136

46 S.G. Harris, M.L. Shuler. Growth of Endothelial Cells on Microfabricated Silicon Nitride Membranes for an In Vitro Model of Blood-Brain Barrier. *Biotechnology and Bioprocess Engineering*, 2003, 8: 246-251

47 K. Jang, K. Sato, K. Igawa, U.I. Chung, T. Kitamori. Development of an Osteoblast-Based 3D Continuous-Perfusion Microfluidic System for Drug Screening. *Analytical Bioanalytical Chemistry*, 2008, 390: 825-832

48 A.J. Engler, S. Sen, H.L. Sweeney, D.E. Discher. Matrix Elasticity Directs Stem Cell Lineage Specification. *Cell,* 2006,126, 645-647

49 D. Huh, H. Fujioka, Y.C. Tung, N. Futai, R. Paine III, J.B. Grotberg, S. Takayama. Acoustically Detectable Cellular-Level Lung Injury Induced by Fluid Mechanical Stresses in Microfluidic Airway Systems. *Proceedings of the National Academy of Sciences of the United States of America*, 2007, 104: 18886-18891

50 D. Huh, B. D. Matthews, A. Mammoto, M. Montoya-Zavala, H. Y. Hsin, D. E. Ingber. Reconstituting Organ-Level Lung Functions on a Chip. *Science,* 2010. 328: 1662 – 1668

51 M.L. Radisic, R.K. Iyer, and S.K. Murthy. Micro-and nanotechnology in cell separation. *International Journal of Nanomedicine*, 2006, 1, 3–14

52 N.D. Gallant, K.E. Michael, A.J. García. Cell Adhesion Strengthening: Contributions of Adhesive Area, Integrin Binding, and Focal Adhesion Assembly. *Molecular Biology of the Cell*, 2005, 16, 4329-4340

53 A. Corlu, G. Ilyin, S. Cariou, I. Lamy, P. Loyer, and C. Guguen-Guillouzo. The coculture: a system for studying the regulation of liver differentiation/proliferation activity and its control. *Cell Biologyand Toxicology*, 1997, 13: 235-242

63

54 K. Kulig, J.P. Vacanti. Hepatic Tissue Engineering. *Transplant Immunology,* 2004, 12, 303-310

55 K. Ohashi, T. Yokoyama, M. Yamato, H. Kuge, H. Kanehiro, M. Tsutsumi, T. Amanuma, H. Iwata, et al. Engineering functional two-and three-dimensional liver systems in vivo using hepatic tissue sheets. *Nature Medicine,* 2007, 13: 880-885

56 P.J. Lee, P.J. Hung, L.P. Lee. An Artificial Liver Sinusoid With a Microfluidic Endothelial-Like Barrier for Primary Hepatocyte Culture. *Biotechnology and Bioengineerin,.* 2007, 97: 1340-1346

57 N. Gueven, B. Glatthaar, H.G. Manke, H. Haemmerle. Co-cultivation of rat pneumocytes and bovine endothelial cells on a liquid-air interface. *European Respiratory Journal*, 1996, 9: 968-75

58 M.I. Hermanns, R.E. Unger, K. Kehe, K. Peters, C.J. Kirkpatrick. Lung epithelial cell lines in coculture with human pulmonary microvascular endothelial cells: development of an alveolo-capillary barrier in vitro. *Laboratory Investigations*, 2004, 84: 736-52

59 S. Duncanson, T. Kniazeva, M.E. Keegan, G.E. Owens, R. Soong, et al. Functionalized Microfluidic Networks for Evaluation of Vascular Injury TEMIS - NA 2008 Conference & Expo; December 7-10; San Diego, CA 2008

60 S.H. Ma, L.A. Lepak, R.J. Hussain, W. Shain, M.L. Shuler. An endothelial and astrocyte co-culture model of the blood-brain barrier utilizing an ultra-thin, nanofabricated silicon nitride membrane. *Lab on Chip*, 2005, 5: 74-85

61 J. Shao, L. Wu, J. Wu, Y. Zheng, H. Zhao, X. Lou, et al. A microfluidic chip for permeability assays of endothelial monolayer. *Biomedical Microdevices*, 2010, 12: 81-88

62 K.J. Jang, K.Y. Suh. A multi-layer microfluidic device for efficient culture and analysis of renal tubular cells. *Lab on Chip*, 2010, 10: 36-42

63 M.Y. Lee, R.A. Kumar, S.M. Sukumaran, M.G. Hogg, D.S. Clark, J.S. Dordick. Three-dimensional cellular microarray for high-throughput toxicology assays. *Proceedings of the National Academy of Sciences*, 2008, 105: 59-63

64 H. Becker, C. Gärtner. Polymer Microfabrication Technologies for Microfluidic Systems. *Analytical and Bioanalytical Chemistry*, 2008, 390: 89-111

65 U.M. Attia, S. Marson, J.R. Alcock. Micro-Injection Moulding of Polymer Microfluidic Devices. *Microfluidics and Nanofluidics*, 2009, 7: 1-28

66 T.C. Merkel, V.I. Bondar, K. Nagai, B.D. Freeman, I. Pinnau. Gas sorption, diffusion, and permeation in poly(dimethylsiloxane). *Journal of Polymer Science Part B: Polymer Physic,* 2000, 38, 415 – 434

67 A. Piruska, I. Nikcevic, S.H. Lee, C. Ahn, W.R. Heineman, P.A. Limbach, C.J. Seliskar. The autofluorescence of plastic materials and chips measured under laser irradiation. *Lab on a Chip*, 2005, 5, 1348-1354

68 K. S. Lee, R. J. Ram. Plastic–PDMS bonding for high pressure hydrolytically stable active microfluidics. *Lab on a Chip*, 2009, 9: 1618–1624

69 J.C. McDonald, D.C. Duffy, J.R. Anderson, D.T. Chiu, H. Wu, O.J.A. Schueller, G.M. Whitesides. Fabrication of microfluidic systems in poly(dimethylsiloxane). *Electrophoresis*, 2000, 1: 27-40

70 C.W. Yung, J. Fiering, A.J. Mueller, D.E. Ingber. Micromagnetic-microfluidic blood cleansing device. *Lab on Chip*, 2009, 9: 1171-1177

71 K. Aran, L.A. Sasso, N. Kamdar and J.D. Zahn. Irreversible, direct bonding of nanoporous polymer membranes to PDMS or glass microdevices. *Lab on Chip*, 2010, 10: 548-552

72 M. Zhang, J. Wu, L. Wang, K. Xiao, W. Wen. A simple method for fabricating multi-layer PDMS structures for 3D microfluidic chips. *Lab on Chip*, 2010, 10: 1199-1203

Appendices

Appendix A: PDMS Spin Curve Data

Table A- PDMS spin speed (RPM) versus PDMS thickness results (µm)

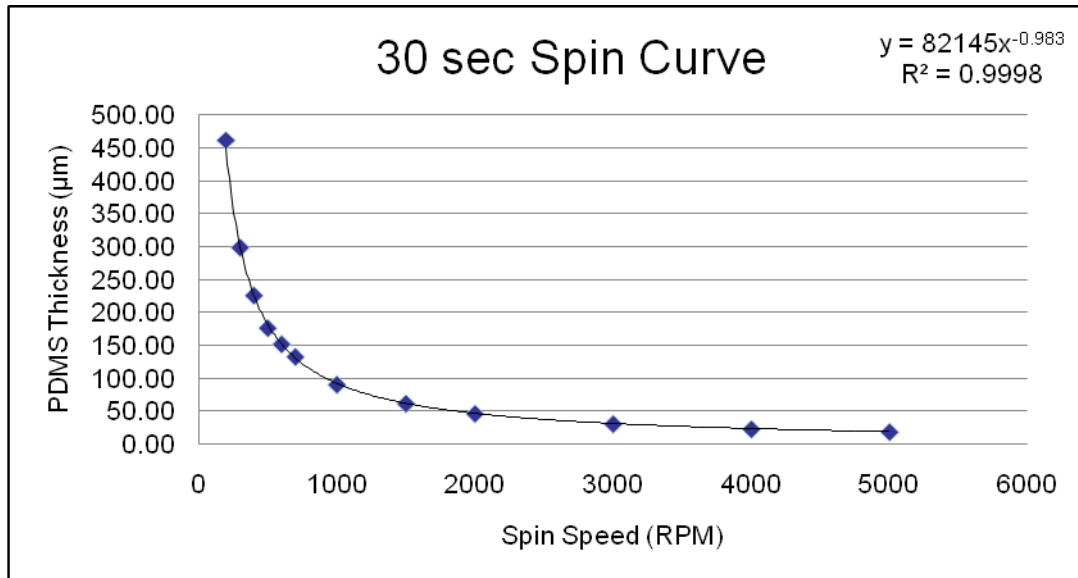| Spin Speed	Thickness Result
200	461.95
300	299.53
400	226.79
500	177.17
600	152.62
700	133.52
1000	91.33
1500	62.45
2000	47.04
3000	31.37
4000	23.53
5000	19.23

Figure A- Graph of PDMS spin speed versus PDMS thickness measurements

67

Appendix B: APTES Bonding Optimization

	Polycarbonate 3µm PVPF	Polycarbonate 3µm PVP Treated	Polyester 10µm PVP-not indicated
Wet Membrane	✓	✓	✓
Dried Membrane	✓	✓	✓

Figure B- PDMS bonding to membranes

	Polycarbonate 3µm PVPF	Polycarbonate 3µm PVP Treated	Polyester 10µm PVP-not indicated
Wet Membrane	✓	✓	✓
Dried Membrane	✓	✗	✗

Figure C- Glass bonding to membranes

Appendix C: Cell Culture and Imaging Protocol

(Courtesy of Steven Maher)

For seeding, the cells were trypsin treated, harvested, pumped into the device and held static for 1 hour, allowing the cells to attach to the collagen coated membrane. After seeding devices were perfused through the chamber opposite that of cells at 90 µl/hr. Stains were diluted to media as follows: rhodamine phalloidin: 100nM, Hoechst 33342: 10 ng/ml. Mitotracker™ Red: 500nM. Approximately 1 hr after addition of stain to media, cells showed strong flourescence and were imaged with a 100x oil objective on a DeltaVision Core with Weather Station (Applied Precision, Issaquah, Washington). Images were taken as a Z stack through the entire verticle axis of target cells and were deconvoluted using softWoRX® Suite (Applied Precision) where mitocondia was able to be distinguished.